SCIENCE CHINA Materials

REVIEWS

mater.scichina.com link.springer.com

Published online 31 January 2018 | https://doi.org/10.1007/s40843-017-9151-y

Sci China Mater 2018, 61(6): 771–805

SPECIAL ISSUE: Advanced Materials for Photoelectrochemical Cells

Recent progress on advanced design for photoelectrochemical reduction of CO_2 to fuels

Ning Zhang, Ran Long, Chao Gao* and Yujie Xiong*

ABSTRACT **The energy crisis and global warming become severe issues. Solar-driven CO_2 reduction provides a promising route to confront the predicaments, which has received much attention. The photoelectrochemical (PEC) process, which can integrate the merits of both photocatalysis and electrocatalysis, boosts splendid talent for CO_2 reduction with high efficiency and excellent selectivity. Recent several decades have witnessed the overwhelming development of PEC CO_2 reduction. In this review, we attempt to systematically summarize the recent advanced design for PEC CO_2 reduction. On account of basic principles and evaluation parameters, we firstly highlight the subtle construction for photocathodes to enhance the efficiency and selectivity of CO_2 reduction, which includes the strategies for improving light utilization, supplying catalytic active sites and steering reaction pathway. Furthermore, diversiform novel PEC setups are also outlined. These exploited setups endow a bright window to surmount the intrinsic disadvantages of photocathode, showing promising potentials for future applications. Finally, we underline the challenges and key factors for the further development of PEC CO_2 reduction that would enable more efficient designs for setups and deepen systematic understanding for mechanisms.**

Keywords: photoelectrocatalysis, CO_2 reduction, light utilization, semiconductor, selectivity

INTRODUCTION

The gargantuan consumption of fossil resources calls for urgent development of clean and renewable energy. Due to the limitless supply and easy acquirement, solar energy exhibits splendid talents as the most attractive alternative energy source [1–6]. Tremendous efforts have been focused on photoelectrochemical (PEC) [7–9] and photocatalytic water splitting [10–12] for maximizing the utilization efficiency of solar energy, which generally employs semiconductors as light-harvesting antennas. Considering the excessive emission of atmospheric carbon dioxide (CO_2) caused by the combustion of fossil fuels, the sunlight-driven CO_2 reduction into higher energy chemicals, such as carbon monoxide, formic acid, methanol or methane, offers a more promising approach to alleviate both global warming and energy crisis [13–17]. Since the pioneering research for photocatalytic CO_2 reduction using a series of semiconductor powders in water was reported in 1979 [18], the development of photocatalysts for CO_2 reduction has been explored with great efforts. Nowadays, a large number of heterogeneous and homogeneous photocatalysts have been enormously exploited and optimized to improve the efficiency of CO_2 reduction [13,19]. Despite the tremendous achievements, direct CO_2 photo-reduction is still believed to be challenging because CO_2 molecule has a stable thermodynamic configuration and a high energy barrier impeding its activation and conversion. Meanwhile, the reaction processes are multistep and complicated, indicating the difficulty of maneuvering the products [15]. For this reason, their conversion efficiency and selectivity are largely limited.

Compared with photocatalytic process, photoelectrocatalysis, which integrates photocatalysis with eletrocatalysis, can utilize external voltage to overcome the energy barrier and to compensate the potential deficiency, achieving higher efficiency for solar conversion [7,20]. Glorious successes have been fulfilled for PEC water splitting in recent years, including both hydrogen pro-

Hefei National Laboratory for Physical Sciences at the Microscale, iChEM (Collaborative Innovation Center of Chemistry for Energy Materials), School of Chemistry and Materials Science, and National Synchrotron Radiation Laboratory, University of Science and Technology of China, Hefei 230026, China

* Corresponding authors (emails: yjxiong@ustc.edu.cn (Xiong Y); gaoc@ustc.edu.cn (Gao C))

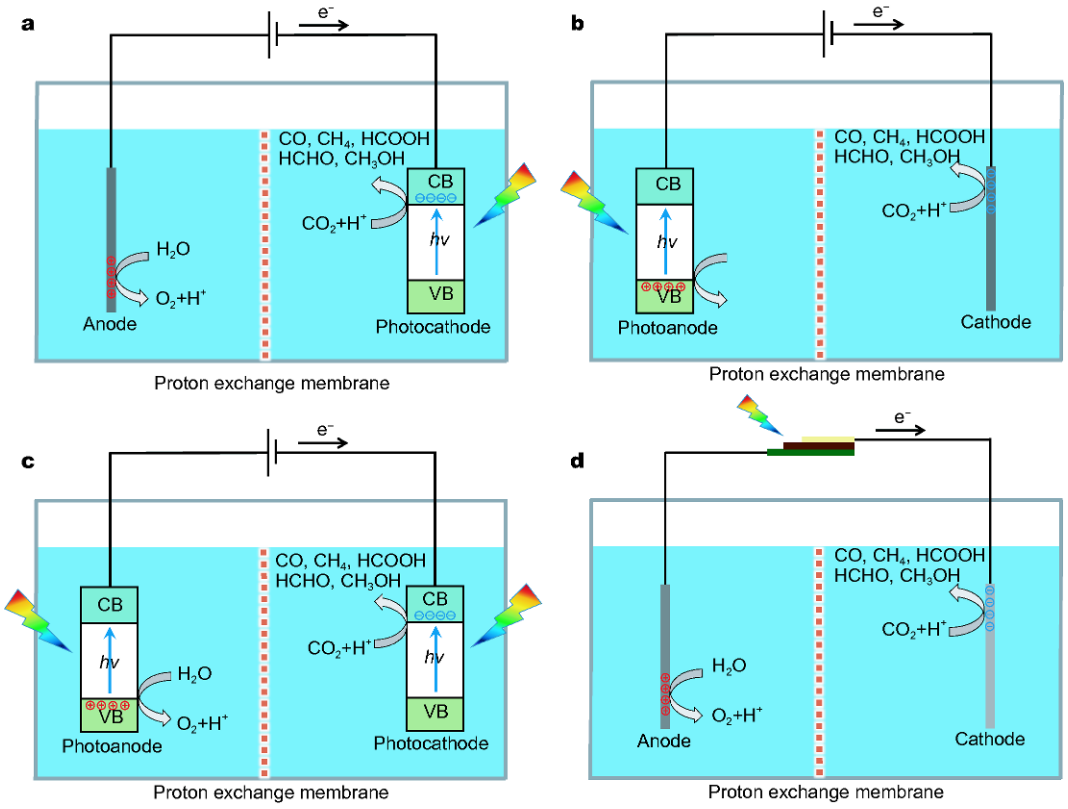

Figure 1 Schematic diagrams for PEC CO_2 reduction in water using semiconductor as (a) photocathode, (b) photoanode and (c) both photoanode and photocathode. (d) Schematic diagram for the device combining a photovoltaic cell with an efficient electrochemical catalyst for CO_2 reduction.

duction [21,22] and oxygen evolution [23,24]. In the PEC system, differently from the traditional electrocatalysis which commonly uses metals as electrodes, semiconductors are commonly manufactured into photoelectrodes in order to harvest solar energy and catalyze the reactions [25]. Several distinct merits are embodied in the PEC system: 1) the applied external electrical bias drives the migration and aggregation of photogenerated electrons and holes at cathode and anode, respectively, which can efficiently suppress their combination; 2) the PEC cells usually separate the anode and cathode, avoiding the mixture of oxidative and reductive products; 3) from the viewpoint of electrochemical catalysis, the photoelectrocatalysis utilizing solar energy can supply additional charges and significantly reduce electricity consumption while the powerful electric force endows high efficiency. Given the merits, it is regarded that photoelectrocatalysis is an efficacious strategy for CO_2 reduction. In 1978, Halman firstly reported the PEC reduction of CO_2 to HCOOH, HCHO and CH_3OH, using p-GaP as photocathode with an external electrical bias [26]. Since then, unremitting explorations have been implemented and this research field has received increasing attention in recent years [13,27,28].

The principles of light harvesting and setup for PEC CO_2 reduction are similar to those for water splitting [8,13]. Briefly, the photoelectrode is immersed into the electrolyte solution. Under light illumination, the incident photons with energy equal to or higher than the band gap energy (E_g) of photoelectrode can be absorbed to excite electrons from valence band (VB) to conduction band (CB) and simultaneously generate holes in VB. With the assist of external electrical bias, the photogenerated electrons and holes migrate to and accumulate at the surface of cathode and anode, respectively. Finally, the photogenerated electrons reduce CO_2 into fuels, while the holes oxidize H_2O into O_2 or react with sacrificial agents. However, it is notable that the reduction of protons into H_2 usually occurs and competes with CO_2 reduction in protonic solvent such as water, which largely limits the efficiency and selectivity of CO_2 reduction [15].

As a reduction reaction, CO_2 conversion is carried out on the surface of cathode in the electrochemical cell. As a matter of fact, the common strategy for PEC CO_2 re-

Table 1 Thermodynamic reactions of CO_2 reduction [49]

Equation	Reaction	ΔH^0 (kJ mol^{-1})	ΔG^0 (kJ mol^{-1})	ΔE^0 (V)
1	$CO_2(g) \rightarrow CO(g) + 1/2O_2(g)$	283	257	1.33
2	$CO_2(g) + H_2O(l) \rightarrow HCOOH(l) + 1/2O_2(g)$	270	286	1.48
3	$CO_2(g) + H_2O(l) \rightarrow HCHO(l) + O_2(g)$	563	522	1.35
4	$CO_2(g) + 2H_2O(l) \rightarrow CH_3OH(l) + 3/2O_2(g)$	727	703	1.21
5	$CO_2(g) + 2H_2O(l) \rightarrow CH_4(g) + 2O_2(g)$	890	818	1.06
6	$H_2O(l) \rightarrow H_2(g) + 1/2O_2(g)$	286	237	1.23

duction is to construct the photocathodes using p-type semiconductors (Fig. 1a). Numerous p-type semiconductors have been exploited and investigated, including silicon [29,30], metal oxides [31–33], sulfides [34,35], tellurides [36,37], phosphides [38,39] and others [40,41]. In addition, profiting from the remarkable activity for CO_2 adsorption and activation, metal materials (e.g., Pd, Au, Ag and Cu) usually serve as the cathodes in electrochemical CO_2 reduction [42]. As such, another promising approach to PEC CO_2 reduction is to employ an efficient catalyst for electrochemical CO_2 reduction as cathode and to utilize photoanode for harvesting solar energy and providing photogenerated electrons (Fig. 1b) [43,44]. The two methods are both to utilize photoelectrodes for harvesting light. To maximize the light absorption and suit for both CO_2 reduction and H_2O oxidation, a PEC cell combining photoanode with photocathode has also been developed for CO_2 reduction (Fig. 1c) [45,46]. Recently, a novel tandem device coupling a photovoltaic cell for photoelectrical conversion with an efficient electrocatalyst for catalysis has been developed for CO_2 reduction (Fig. 1d), also demonstrating the excellent efficiency and promising potential [47,48].

Upon the tremendous efforts on photocatalytic CO_2 reduction, several excellent reviews which mainly focus on elucidating the design philosophy of photocatalysts and/or the modulation strategies for reaction pathways have been reported [13–17]. Although photoelectrocatalysis has exhibited attractive prospect for CO_2 reduction, few reviews can be referred and most of them are outlined only as a section of photocatalysis [27,28]. In this review, we will systematically outline the recent developments for PEC CO_2 reduction, including the precious material designs of photoelectrodes and the modulation of reaction pathway. Firstly, the fundamentals for PEC CO_2 reduction will be introduced, which enables readers roughly to understand the basic principles for CO_2 reduction, including thermodynamics and kinetics, matters of external reaction conditions and evaluation parameters. Secondly, we will summarize the diversiform approaches to construct photocathode with efforts to improve the efficiency and selectivity of CO_2 reduction, such as tuning light harvesting, steering charge kinetics, maintaining electrode stability, facilitating CO_2 activation, maneuvering reaction pathways and suppressing undesired products. Thirdly, other novel developed setups for PEC CO_2 reduction will be outlined and discussed. Finally, we will preliminarily assess the merits of present strategies for PEC CO_2 reduction and propose the remaining challenges and future prospects.

BASIC PRINCIPLES FOR PEC CO_2 REDUCTION

Thermodynamics and kinetics of CO_2 reduction

CO_2 molecule contains two C=O bonds with a linear configuration. The orbitals of C atom are sp-hybridized, forming two σ bonds with O atoms, while the other two nonhybridized p orbits in C atom form two π_3^4 bonds with the p orbits in O atoms. As a result, the C=O bonds are extremely stable and have a dissociation energy as high as ~750 kJ mol^{-1}, which indicates that a high activation barrier must be overcome for CO_2 activation and C=O bond cleavage. Moreover, given the highest chemical state (+4) of C atom in CO_2, the reduction of CO_2 can result in complex products including CO, HCOOH, HCHO, CH_3OH and CH_4, etc. [15]. The standard enthalpy (ΔH^0), Gibbs free energy (ΔG^0) and redox potential (ΔE^0) of CO_2 reduction are summarized in Table 1 [49]. All of the CO_2 reduction processes are more highly endothermic than water splitting owing to the positive ΔG^0 values, particularly for hydrocarbon fuels such as CH_3OH and CH_4, indicating that CO_2 reduction is more thermodynamically unfavorable at ambient temperature.

The thermodynamic redox potentials for various CO_2

Table 2 The thermodynamic potentials *versus* the normal hydrogen electrode (NHE) at pH 7 for various CO_2 reduction products and water splitting [50,51]

Equation	Products	Reaction	ΔE^0 (V) *vs.* NHE at pH 7
7	$CO_2^{\bullet-}$ intermediate	$CO_2 + e^- \rightarrow CO_2^{\bullet-}$	−1.9
8	Carbon monoxide	$CO_2 + 2H^+ + 2e^- \rightarrow CO + H_2O$	−0.53
9	Formic acid	$CO_2 + 2H^+ + 2e^- \rightarrow HCOOH$	−0.61
10	Formaldehyde	$CO_2 + 4H^+ + 4e^- \rightarrow HCHO + H_2O$	−0.48
11	Methanol	$CO_2 + 6H^+ + 6e^- \rightarrow CH_3OH + H_2O$	−0.38
12	Methane	$CO_2 + 8H^+ + 8e^- \rightarrow CH_4 + 2H_2O$	−0.21
13	Hydrogen	$2H^+ + 2e^- \rightarrow H_2$	−0.41
14	Oxygen	$H_2O + 2h^+ \rightarrow 1/2O_2 + 2H^+$	0.82

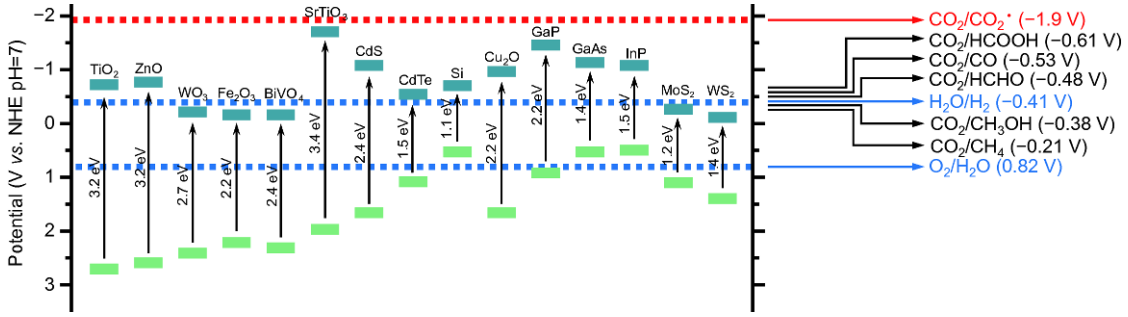

Figure 2 Conduction band and valence band potentials of several typical semiconductors relative to the standard redox potentials of CO_2 reduction in water at pH 7.

reduction products and water splitting are listed in Table 2 [50,51]. The first step of CO_2 reduction may undergo the one-electron reduction to $CO_2^{\bullet-}$ intermediate [52]; however, this reaction is extremely thermodynamically unfavorable due to the highly negative redox potential (Equation 7) of −1.9 V *versus* the normal hydrogen electrode (NHE) at pH 7, which is generally regarded as the rate-limiting step. Fig. 2 outlines the CB and VB potentials of some typical semiconductors relative to the standard redox potential of various products. The CB edges of all listed semiconductors are located below the redox potential of $CO_2^{\bullet-}$ intermediate, suggesting that this one-electron reduction process is thermodynamically unfavorable and can hardly be triggered without external force.

On the other hand, the redox potentials of multiple electron reduction processes (Equations 8–12) are close to that of H_2 generation. These processes generally involve the participation of protons, called proton-coupled electron transfer (PCET) process [53]. The PCET processes can bypass the generation of thermodynamically unfavorable $CO_2^{\bullet-}$ and have a lower energy barrier to carry out. However, the multiple electron transfer reactions usually suffer from kinetic limits [54]. For instance, although the higher redox potential of CH_4 formation (Equation 12) than H_2 generation implies that the formation of CH_4 is more thermodynamically favorable, eight electrons and eight protons need to participate in the reaction of forming CH_4, which is more difficult than the two-electron induced H_2 generation. Furthermore, the PCET processes always involve multistep reactions [14]. Despite the yet ambiguous mechanism, two plausible pathways for CO_2 reduction to CH_4 are extensively studied and partially verified: formaldehyde pathway [55] and carbene pathway [56] (Fig. 3). The intermediates could desorb into solvent to form the side products during the reaction processes. For instance, HCOOH and HCHO could be generated in the formaldehyde pathway (Fig. 3a) while CO is the main side-product for carbene pathway (Fig. 3b). In addition, some other pathways involving C–C coupling (e.g., glyoxal pathway) were also reported and investigated, which might induce more complicated products [57]. The products are sensitively influenced by photocatalysts and external environments during the processes of reduction, forming a grand challenge for optimizing the selectivity of CO_2 reduction.

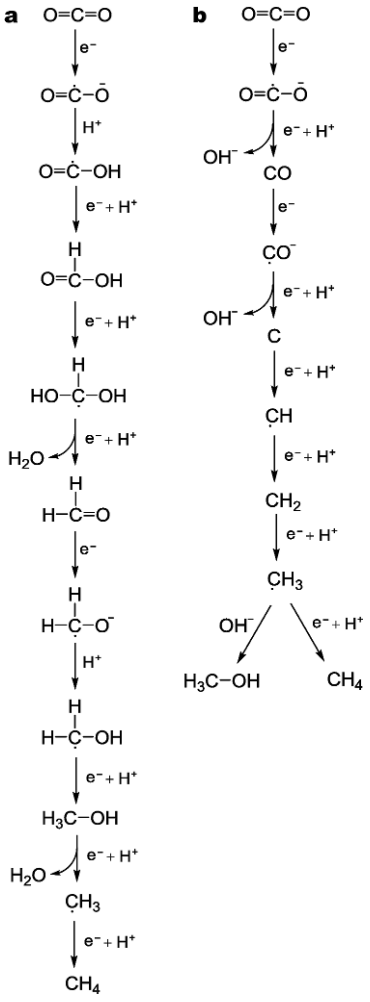

Figure 3 Two proposed mechanisms for CO_2 reduction to methane: (a) formaldehyde pathway and (b) carbene pathway. Reproduced with permission from Ref. [14]. Copyright 2013, Wiley-VCH Verlag GmbH & Co.

Specifically in the case of PEC CO_2 reduction, an external electrical bias is commonly applied so as to largely satisfy the thermodynamic matters. The overall efficiency can be improved by maneuvering reaction kinetics. The impending challenge is how to efficaciously improve the electron utilization, activate CO_2 molecules and maneuver the products [27]. Recently, unremitting endeavors have been put based on the subtle material designs for photoelectrocatalysis and the modulation of reaction pathways, which will be outlined and discussed in the following sections.

Matters of external reaction conditions

The pathways for CO_2 reduction are complicated, which can be susceptibly affected by the external reaction conditions such as external bias, reaction temperature and pressure, electrolyte pH value and solvent composition [13,42]. The alteration of external conditions can tune the state of CO_2 molecules and the adsorption of various products, thereby impacting on the efficiency and products of CO_2 reduction.

Reaction temperature and pressure

The reaction temperature typically has a distinct impact on CO_2 reduction. It is well recognized that high temperature reduces the solubility of CO_2 in solvent, which generally leads to a subsequent decrease in production [13]. For this reason, some studies specifically performed photocatalysis using cooling water systems to avoid the increase of reaction temperature [58,59]. Moreover, the selectivity of products can also be altered by the reaction temperature, owing to the different adsorption ability of products [60]. For instance, Cook *et al.* [61] investigated the products of PEC CO_2 reduction using Cu-loaded p-SiC at various temperature, and identified that methanation occurred only in a temperature range of 30–60°C.

In addition to temperature, the pressure of CO_2 also affects the solubility. High-pressure environment can increase the CO_2 concentration in solution, endowing higher PEC current density and CO_2 conversion rate [62,63]. Moreover, it was reported that high CO_2 pressure could also facilitate the CO_2 reduction *versus* proton reduction and enhance the stability of photocathode [62,63].

pH value

The pH value of electrolyte plays a critical role in altering reaction pathways and final products. In an aqueous solution, the dissolved CO_2 molecules can undergo hydration to form carbonic acid (H_2CO_3) and might dissociate into bicarbonate (HCO_3^-) or carbonate (CO_3^{2-}). The ratios of H_2CO_3, HCO_3^- and CO_3^{2-} to molecular CO_2 are determined by the pH of solution [64]. At pH < 4.5, H_2CO_3 can hardly dissociate so that it and molecular CO_2 dominantly exist. HCO_3^- is the major component at pH between 4.5–8.5. As pH is higher than 8.5, H_2CO_3 is completely hydrolyzed to form CO_3^{2-}. The different chemical species are adsorbed on the surface of catalyst through various configurations, which can determine the preferential reaction pathways and final products [65].

Moreover, as mentioned in Section "Thermodynamics and kinetics of CO_2 reduction", PCET involves the participation of protons, indicating that a high proton concentration favors the PCET process. However, the proton reduction for H_2 evolution is significantly enhanced at

low pH value due to the advantages of kinetics [66], which competes with CO_2 reduction to cause low selectivity and Faradaic efficiency. As a result, most catalytic experiments are performed in a neutral or basic solution.

Solvent

Water is the most widely used solvent for PEC CO_2 reduction as well as serves as the proton source [32,36]. However, the solubility of CO_2 in water is quite low (i.e., 0.033 mol L^{-1} at 25 °C under 1 atm) [67], which disfavors the adsorption of CO_2 to catalysts and largely suppresses the reduction process. It has been reported that CO_2 molecules are substantially more soluble in non-aqueous organic solvents [68]. For instance, the solubility of CO_2 in methanol is nearly 5 times higher than that in water under ambient conditions. Benefiting from the outstanding solubility, many organic solvents including methanol [69], acetonitrile [33] and *N*,*N*-dimethylformamide (DMF) [70] also serve as the electrolyte for PEC CO_2 reduction. In this case, the predominant product of CO_2 reduction is CO due to the absence of protons. To enable the PCET process, sacrificial donors (e.g., triethylamine (TEA) and triethanolamine (TEOA)) are added to consume the holes and supply protons. In parallel, water can also be taken as the proton donor in non-aqueous solvent, as a trace amount of water can hardly influence the solubility.

In addition to organic solvents, ionic liquids have excellent capture capacity for CO_2 through the coordination with CO_2 molecules, emerging as the solvent with the promising potential for CO_2 reduction. The ionic liquids have been well utilized in electrocatalysis [71] and photocatalysis [72]. Moreover, it has been revealed that the unique coordination configuration with ionic liquids can lower the energy barrier of $CO_2^{\bullet-}$ intermediate, facilitating the reduction of CO_2 [73]. Recently, this merit has been applied to the PEC CO_2 reduction. The utilization of ionic liquid (i.e., 1-aminopropyl-3-methylimidazolium bromide) significantly promotes the conversion of CO_2 to HCOOH and suppresses the competitive hydrogen evolution [74].

External bias

To facilitate the reduction of CO_2, external bias is generally applied to supply sufficient electrons for enhancing the efficiency of CO_2 conversion. Similar to electrocatalysis, the applied external bias has a distinct effect on the selectivity of CO_2 reduction, especially competing with water reduction. The varied external bias, which can alter the electron transfer and energy barrier during the reduction process, endows different power for reduction.

In general, the selectivity of CO_2 reduction exhibits a volcanic type for electrocatalysis with the increase of external bias [42]. As such, an optimal external bias can be identified to obtain the highest selectivity. However, in terms of photoelectrocatalytic process, it seems no law to follow as many factors play their roles in the overall selectivity. For instance, the selectivity of CO_2 reduction to CO increased with the applied external bias by using the ZnTe/ZnO film as a photocathode [36]. However, when coupled with Au nanoparticles, the selectivity showed a volcanic type and could be optimized at an external bias of −0.5 V *versus* reversible hydrogen electrode (RHE) under the same reaction condition [37]. Given this situation, it is suggested that the relationship between external bias and selectivity should be examined to identify the optimal external bias for CO_2 reduction.

Evaluation parameters for PEC CO_2 reduction

Based on the combination of photocatalysis and electrocatalysis, the evaluation parameters for both can be employed for the assessment of PEC CO_2 reduction.

Product evolution rate and catalytic current density

The product evolution rate is generally normalized over the mass of catalyst or the effective area of photoelectrode (i.e., μmol h^{-1} g_{cat}^{-1} or μmol h^{-1} cm^{-2}). Similarly, the catalytic current density is usually normalized by the area of photoelectrode at the desired potential *versus* reference electrode (i.e., mA cm^{-2} *vs.* RE). The values for product evolution rate and current density together denote the performance of PEC CO_2 reduction.

Turnover number and turnover frequency

Turnover number (TON) and turnover frequency (TOF) can well evaluate the activity of catalytic active centers, which have been extensively applied to metal nanoparticles and homogeneous metal complex catalysts. The definitions for PEC CO_2 reduction are listed below (Equations 15, 16) [33].

$$\mathrm{TON} = \frac{n_{\mathrm{product}}}{n_{\mathrm{catalyst}}}, \tag{15}$$

$$\mathrm{TOF} = \frac{n_{\mathrm{product}}}{n_{\mathrm{catalyst}} \times t}, \tag{16}$$

where n_{product} and n_{catalyst} are the molar numbers of desired products and catalysts, respectively, and t is the reaction time.

Quantum yield

Quantum yield (QY) is a crucial parameter for assessing the performance of photocatalyst. The internal and apparent quantum yields are defined by Equations 17, 18, respectively [10].

$$\text{Internal quantum yield} = \frac{\alpha \times n_{\text{product}}}{n_{\text{photon}}} \times 100\%, \quad (17)$$

$$\text{Apparent quantum yield} = \frac{\alpha \times n_{\text{product}}}{n'_{\text{photon}}} \times 100\%, \quad (18)$$

where α is the number of needed electrons for product evolution (e.g., 2 for CO and 8 for CH_4), n_{product} is the number of desired products, and n_{photon} and n'_{photon} are the number of absorbed and incident photons, respectively.

Faradaic efficiency

On account of various products, the selectivity is an indispensable parameter for the evaluation of CO_2 reduction. In terms of photoelectrocatalysis, the Faradaic efficiency (FE) is typically used to assess the efficiency of producing selective products and calculated by Equation 19 [42].

$$\text{FE} = \frac{\alpha \times n_{\text{product}} \times F}{Q}, \quad (19)$$

where α is the number of needed electrons for product evolution, n_{product} is the molar number of desired products, F is the Faraday's constant, and Q is the total passed charge.

ADVANCED DESIGNS OF PHOTOCATHODES FOR PEC CO_2 REDUCTION

The most common setup for PEC CO_2 reduction is composed of a semiconductor photocathode and a counter anode (e.g., Pt or carbon material). The photocathode harvests light to provide electrons and holes for catalysis. Given the mechanisms, light utilization can be essentially improved by enhancing light harvesting and steering charge kinetics, which eventually boosts the catalytic activity of CO_2 reduction [17]. To this end, tremendous efforts have been made to design the architectures for photocathodes.

In addition to light utilization, the major challenges and limits for highly efficient solar-driven CO_2 reduction are the unfeasible CO_2 activation, complicated reaction pathways and uncontrollable reduction products [15]. However, semiconductor photocathodes often show the frustrating activity in CO_2 reduction due to the deficiency of active sites for CO_2 activation. It is a promising strategy for effectively surmounting this predicament that highly efficient catalysts such as metal nanoparticles [75,76] and homogeneous metal complexes [21,34,46] as co-catalysts are anchored on the surface of photocathodes. The involvement of co-catalysts can facilitate CO_2 activation, modulate reaction pathways and maneuver desirable products, which have been extensively applied to PEC CO_2 reduction. In this section, we will emphatically outline the recent advanced designs of photocathodes for improving the efficiency of CO_2 reduction.

Designing unique structures for photocathodes

In photocatalysis and photoelectrocatalysis, the light utilization, including light harvesting, charge separation and migration, is prerequisite to the subsequent catalytic reactions [77]. In terms of PEC CO_2 reduction, efficient light utilization should be firstly guaranteed to deliver sufficient electrons for the reactions. However, traditional photocathodes suffer from inferior light harvesting, serious charge combination and/or slow electron migration. To overcome those challenges, tremendous efforts have been implemented. Designing the unique geometrical and electronic structures for photocathodes is a competent approach to improve light harvesting and steer charge kinetics [22,25]. Some recently reported advances for designing the unique structures for photocathodes are summarized in Table 3.

Utilizing one-dimensional nanostructures

Profiting from their unique geometrical and electronic characteristics, one-dimensional (1D) nanostructures exhibit widespread applications in PEC water splitting and promising potentials in CO_2 reduction [78,79]. In 1D nanostructures, the electronic wave-function is restricted in nanoscale directions, resulting in the quantum confinement effect. Compared with bulk materials, the physical properties of 1D nanostructures are largely altered by the quantum confinement, which in turn has a profound effect on their light utilization [80]. Furthermore, the intrinsic high length-to-diameter ratio of 1D nanostructures can enhance light absorption and shorten length of electron migration, inducing high incident photontoelectron conversion efficiency [81].

Several semiconductors have been successfully shaped into the 1D nanostructures that serve as photocathodes for PEC CO_2 reduction. A typical case was the fabrication of p-type silicon (p-Si) into nanowire arrays (Fig. 4a–c) [29]. In comparison with planar p-Si photocathodes, 1D

Table 3 Some recently developed advances of photocathodes for PEC CO_2 reduction

Photocathode	Condition	Main products	Efficiency	Ref.
Designing nanostructures for photocathodes				
p-Si nanowire arrays	$KHCO_3$ (0.1 mol L^{-1}), −1.5 V *vs.* SCE, AM 1.5G light (100 mW cm^{-2}), 3 h	CO, formate	4.3 μmol, FE: 7.3% 4.7 μmol, FE: 7.8%	[29]
CuO-Cu_2O nanorod arrays	CO_2-saturated Na_2SO_4 (0.1 mol L^{-1}), −0.2 V *vs.* SHE, AM 1.5G light, 90 min	CH_3OH	ca. 85 mmol L^{-1}, FE: 94–96%	[82]
Cu-decorated Co_3O_4 nanotube arrays	CO_2-saturated Na_2SO_4 (0.1 mol L^{-1}), −0.9 V *vs.* SCE, visible light, 8 h	Formate	6.75 mmol L^{-1} cm^{-2}, select.: close to 100%	[76]
ZnTe coated Zn/ZnO nanowires	$KHCO_3$ (0.5 mol L^{-1}), −0.7 V *vs.* RHE, >420 nm (490 mW cm^{-2}), 1 h	CO	ca. 70 mmol cm^{-1}, FE: 22.9%	[37]
ZnTe/ZnO nanowire arrays	$KHCO_3$ (0.5 mol L^{-1}), −0.7 V *vs.* RHE, AM 1.5G light, 3 h	CO	10.3 μmol cm^{-2}, FE: 7.2% select.: 8.7%	[36]
Polycrystalline Mg-doped $CuFeO_2$	$NaHCO_3$ (0.1 mol L^{-1}, pH=6.8), −0.9 V *vs.* SCE, LED source (470 nm), 8–24 h	Formate	FE: 10%	[95]
Co-doped MoS_2 nanoparticles	$KHCO_3$ (0.1 mol L^{-1}, pH=9), −0.9 V *vs.* SCE, ≥420 nm (100 mW cm^{-2}), 350 min	CH_3OH	35 mmol L^{-1}	[96]
Boron-doped g-C_3N_4 films	$NaHCO_3$ (0.5 mol L^{-1}, pH=7.3), −0.4 V *vs.* Ag/AgCl, AM 1.5G light (100 mW cm^{-2})	C_2H_5OH	5-times larger for photocurrent FE: 78%	[41]
CuO nanowires/Cu_2O/Cu foil	$KHCO_3$ (0.1 mol L^{-1}, pH=6.8), −0.6 V *vs.* RHE, AM1.5 G light, 10 min	CO + HCOOH	1.67 mA cm^{-2}, select.: 60%	[105]
$CuFeO_2$/CuO mixed catalyst	$KHCO_3$ (0.1 mol L^{-1}), no external bias, AM 1.5G light (100 mW cm^{-2})	Formate	5 μmol h^{-1}, select.: 90%, energy efficiency: ~1%	[40]
10 nm TiO_2-passivated p-GaP	NaCl (0.5 mol L^{-1})+pyridine (10 mmol L^{-1}), −0.5 V *vs.* overpotential, green laser (532 nm), 8 h	CH_3OH	0.5 V shift of overpotential 4.9 μmol, FE: 55%	[38]
Anchoring cocatalysts on photocathodes				
Sn-coupled p-Si nanowire arrays	$KHCO_3$ (0.1 mol L^{-1}), −1.5 V *vs.* SCE, AM 1.5G (100 mW cm^{-2}), 3 h	CO, formate	9.8 μmol, FE: 23.0%; 19.5 μmol, FE: 45.5%	[29]
Pb-deposited CuO/Cu_2O film	$KHCO_3$ (0.1 mol L^{-1}), −0.4 V *vs.* SCE, visible light, 1 h	HCOOH, CH_3OH, CO	0.524 μmol h^{-1} cm^{-2}, FE: 19.32% 0.102 μmol h^{-1} cm^{-2}, FE: 11.33% 0.243 μmol h^{-1} cm^{-2}, FE: 9.80%	[75]
Au-coupled ZnTe/ZnO nanowire arrays	$KHCO_3$ (0.5 mol L^{-1}), −0.7 V *vs.* RHE, AM 1.5G light, 3 h	CO	112.0 μmol cm^{-2}, FE: 58.0% Select.: 64.9%	[36]
Re(bipy–*t*Bu)$(CO)_3$Cl+p-Si	CH_3CN/water mixtures, −1.9 V *vs.* Fc/Fc^+, 661 nm, 2.5 h	Syngas (H_2:CO=2:1)	5.6 mA cm^{-2}, FE: 102%	[130]
ZnDMCPP–Re(bpy)(NHAc) complex sensitized p-NiO	Bu_4NBF_4 in DMF solution, Ag/$AgNO_3$ reference, visible light, 5 min	CO	0.93 μmol, FE: 6.3%	[70]
Re(bipy–*t*Bu)$(CO)_3$Cl paired TiO_2-protected Cu_2O	Bu_4NBF_4 (0.1 mol L^{-1}) and CH_3OH (1 mol L^{-1}) in CH_3CN, −1.73 V *vs.* Fc/Fc^+, AM 1.5G light, 5.5 h	CO	1.5 mA cm^{-2}, FE: 100%	[110]
Re(bipy–*t*Bu)$(CO)_3$Cl immobilized mesoporous-TiO_2-modified Cu_2O	Bu_4NBF_4 (0.1 mol L^{-1}) in CH_3CN, −2.05 V *vs.* Fc/Fc^+, AM 1.5G light, 1.5 h	CO	FE: 80–95%	[33]
$[Ru(L\text{-}L)(CO)_2]_n$ polymer modified Zn-doped p-InP	CO_2-saturated water, −0.6 V *vs.* Ag/AgCl, 400<λ<800 nm, 3 h	Formate	0.17 mmol L^{-1}, FE: 62%	[131]
RuCE+RuCA modified $Cu_2ZnSn(S,Se)_4$	CO_2-saturated water, -0.6 V *vs.* Ag/AgCl, 400<λ<800 nm, 3 h	Formate	0.49 mmol L^{-1}, FE: 80%	[34]
Ru(II)-Re(I) supramolecular modified p-type NiO	Et_4NBF_4 (0.1 mol L^{-1}) in DMF/TEOA (5:1, v/v) solution, −1.2 V *vs.* Ag/$AgNO_3$, >460 nm, 3h	CO	255 nmol, TON_{co}: 32 FE: 62% (0–3 h), 98% (3–5 h)	[134]
Fe porphyrin complex modified B-doped p-Si	$[NBu_4][BF_4]$ (0.1 mol L^{-1}) in MeCN/5% DMF (v/v) solution, −1.1 V *vs.* SCE, <650 nm (90 mW cm^{-2}), 6 h	CO	ca. 140 μmol, TON: 175 FE: 80%	[139]
Molecular Mn catalyst immobilized mesoporous TiO_2	Bu_4NBF_4 (0.1 mol L^{-1}) in CH_3CN/H_2O (19:1, v/v) solution, −1.7 V *vs.* Fc/Fc^+, AM 1.5G (100 mW cm^{-2}), 2h	CO	3.75±0.56 μmol, TON: 112±17 FE: 67±5%	[140]
Pyridine+p-$CuInS_2$ films	Na_2SO_4 (0.1 mol L^{-1}, pH 5.2), overpotential of 20 mV, AM 1.5G light (100 mW cm^{-2}), 11 h	CH_3OH	1.2 mmol L^{-1}, FE: 97%	[35]
Pyridine+p-CdTe/FTO	$NaHCO_3$ (0.1 mol L^{-1}) with citric acid buffer (0.1 mol L^{-1}, pH 5), −0.6 V *vs.* SCE, visible light, 6 h	HCOOH	4.19 mA cm^{-2}, 0.167 mmol, FE: 60.7%	[146]
Polypyrrole coated p-CdTe	$KHCO_3$ (0.1 mol L^{-1}, pH 6.7), −0.2 V *vs.* RHE, >420 nm, 6 h	HCOOH, CO	111.1 nmol h^{-1} cm^{-2}, FE: 37.2% 41.1 nmol h^{-1} cm^{-2}, FE: 13.8%	[158]
PMAEMA/CdTe QDs film	$NaClO_4$ (0.1 mol L^{-1}), −0.45 V *vs.* Ag/AgCl, 500 W Xe-Hg lamp, 3 h	HCHO	ca. 5% (μmol HCHO/μmol CO_2)	[159]
CODH functionalized Dye-sensitized p-NiO	MES (0.2 mol L^{-1}, pH 6), −0.27 V *vs.* SHE, visible light	CO	ca. 25 μA cm^{-2}	[32]
Rh-(FDH-FaldDH-ADH) enzymes modified $BiFeO_3$ photocathode	Na_3PO_4 buffer (0.1 mol L^{-1}, pH 7), electrical bias: 0.8 V, >420 nm (150 mW cm^{-2}), 6 h	CH_3OH	220 μmol L^{-1} h^{-1}, 1280 μmol g_{cat}^{-1} h^{-1}	[165]

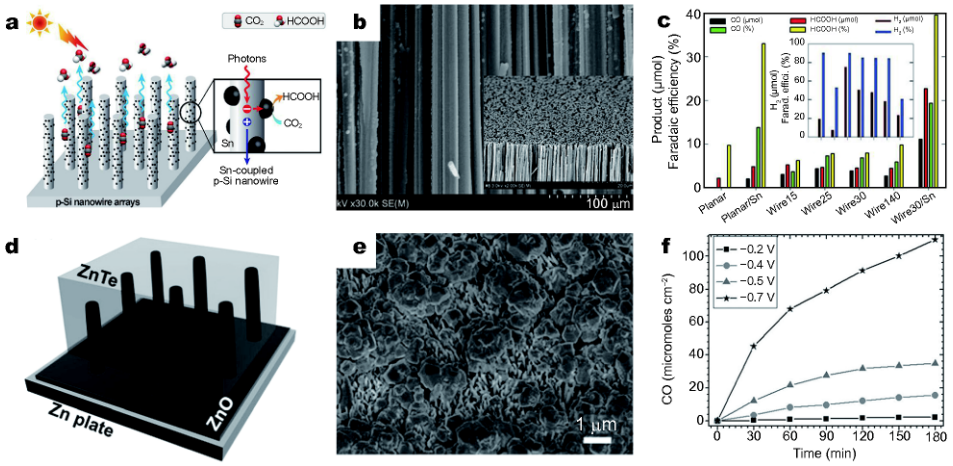

Figure 4 (a) Schematic illustration and (b) SEM image of Sn-coupled p-Si nanowire arrays. (c) Comparison of products and FEs with various p-Si photocathodes. Adapted with permission from Ref. [29]. Copyright 2014, Wiley-VCH Verlag GmbH & Co. (d) Schematic illustration and (e) SEM image of Zn/ZnO/ZnTe structure. (f) The amount of produced CO under different potentials (*vs.* RHE) with Zn/ZnO/ZnTe structure as a photocathode. Adapted with permission from Ref. [37]. Copyright 2014, Wiley-VCH Verlag GmbH & Co.

p-Si nanowire arrays delivered a cathodic onset potential of ca. 0.5 V. After a 3 h reaction, 1D p-Si nanowire arrays produced 4.3 μmol of CO with an FE of 7.3% and formate of 4.7 μmol with an FE of 7.8% at −1.5 V *versus* saturated calomel electrode (SCE), double that observed with planar p-Si. The enhancement was attributed to light trapping and efficient charge transfer in radial directions. In parallel, some p-type metal oxides, such as Cu_2O [82,83] and Co_3O_4 [76], were also designed as 1D nanostructures for photocathodes toward PEC CO_2 reduction. The 1D geometry favored light harvesting and provided more active sites for CO_2 conversion, exhibiting high selectivity and FE for CH_3OH and formate, respectively. Moreover, Lee *et al.* [37] recently reported a photocathode composed of a ZnTe-coated Zn/ZnO nanowire substrate using a simple dissolution-recrystallization method. This photocathode showed a high production rate of ca. 70 mmol cm^{-2} and FE of 22.9% for PEC CO_2 reduction to CO at −0.7 V *versus* RHE after 1 h reaction (Fig. 4d–f).

Doping

Doping is an effective strategy for tuning the electronic properties and light absorption of semiconductor [77]. In terms of intrinsic semiconductor, doping can alter the type of semiconductor. A well-known case is the doped silicon [84]. Doping with N or P element results in n-type properties, while B- or Ga-doped silicon demonstrates p-type characteristics. Moreover, doping with foreign elements can alter the energy band structure and tailor the CB and/or VB position of semiconductor. In general, nonmetal doping can hardly influence CB edge but hybridize VB to shift it upward, which finally narrows the band gap [85].

Differently, doping with metal elements can induce the formation of impurity levels in forbidden band and serve as either an electron donor or an acceptor. The band gap can be narrowed or split into a two-step excitation process by the introduced impurity levels, leading to an obvious redshift of light absorption [86]. The doped metal elements can also modulate the carrier density and conductivity. For instance, the carrier density of recently reported 2% Nb-doped TiO_2 nanowires was up to ~10^{21} cm^{-3}, which was about six orders of magnitude higher than the undoped sample [87]. In addition, the doped metal cations can also act as active sites for reactions, which is beneficial for catalysis. A representative case was the Cu-doped TiO_2 for photocatalytic CO_2 reduction, which exhibited good selectivity of CO_2 conversion to CH_3OH [88]. Another alternative strategy for doping is the self-doping and defect engineering for semiconductor [89–91]. The mechanism for modulating band gaps is quite similar to that by metal doping. A well-known example was the Ti^{3+} self-doped TiO_2 [92], in which the impurity levels introduced by Ti^{3+} were located below CB and performed as an electron trap. It is noteworthy that self-doping and defect engineering can deliver numerous coordinately unsaturated sites (CUSs) for the adsorption and activation of molecules [93,94].

While the doping strategy has been widely applied to the design of photocatalysts, the development of photo-

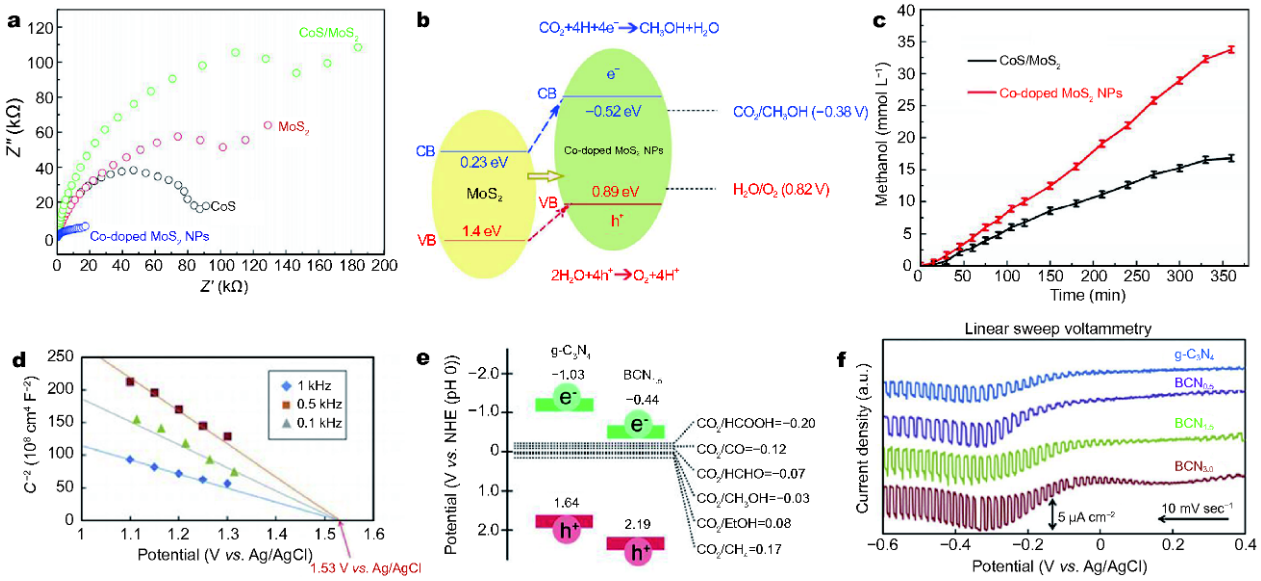

Figure 5 (a) Electrochemical impedance spectroscopy of Co-doped MoS_2, CoS_2, MoS_2 and CoS_2/MoS_2 samples. (b) Mechanism of PEC CO_2 reduction on the Co-doped MoS_2 NPs. (c) Time-dependent curve of methanol yields with Co-doped MoS_2 and CoS_2/MoS_2 samples. Adapted with permission from Ref. [96]. Copyright 2015, Elsevier. (d) Mott-Schottky plot and (e) band potential diagram of B-doped g-C_3N_4 ($BCN_{1.5}$) and (f) photocurrent responses for CO_2 reduction by various B-doped g-C_3N_4 samples. Adapted with permission from Ref. [41]. Copyright 2016, Elsevier.

cathodes for PEC CO_2 reduction is still in preliminary. In 2013, a Mg-doped $CuFeO_2$ delafossite photocathode was fabricated to achieve the PEC reduction of CO_2 to formate [95]. The Mg^{2+} dopant extended the absorption of visiblelight and improved the conductivity of photocathode, offering an FE of 10% at −0.9 V *versus* SCE and an incident photon-to-current efficiency (IPCE) value of 14% at 340 nm using an applied potential of −0.4 V *versus* SCE. Similar results were achieved in the Co-doped MoS_2 nanoparticles (Fig. 5a–c) [96]. The Co element narrowed the band gap, upshifted the CB position and reduced the resistance of MoS_2, which led to the high rate (35 mmol L^{-1} at 350 min) for PEC CO_2 reduction to methanol.

In terms of nonmetal doping, a B-doped g-C_3N_4 (BCN_x) electrode was reported for CO_2 reduction (Fig. 5d–f) [41]. The BCN_x not only significantly altered the energy band structure, but also exhibited an extraordinary p-type conductivity. The photocurrent response of a representative sample (i.e., $BCN_{3.0}$) was about 5 times larger than the undoped g-C_3N_4 sample (Fig. 5f), and the system generated C_2H_5OH as a main product. Decorating the sample with co-catalysts such as Au, Ag or Rh could further enhance the evolution rate of C_2H_5OH but reduce the FE.

Profiting from the modulation of energy band structure and creation of CUSs, self-doping and defect engineering have received more attention in photocatalytic CO_2 reduction [97,98] and PEC water splitting [99]. However, their application in PEC CO_2 reduction was rarely reported. This might result from the less investigation of self-doping and defect engineering in photocathodes. To our delight, several p-type semiconductors were successfully invented by defect engineering to alter their energy band structures and expose numerous CUSs [100,101], which could serve as candidates for photocathode materials toward CO_2 reduction. We anticipate that this approach can endow a new avenue for constructing photocathodes to improve the efficiency of CO_2 reduction.

Forming heterojunctions by semiconductor composites

Limited by the thermodynamics of photocatalysis, the single material system can hardly satisfy all the requirements including light harvesting, redox potential, charge separation and migration. Integrating semiconductors into heterojunctions supplies an effective strategy to surmount those predicaments [102,103]. Several potential merits are embodied by the heterojunctions. 1) Enhancing light absorption. The semiconductor with a wide band gap can be decorated with another component with a narrow band gap, extending the range of light absorption like sensitization. 2) Steering charge kinetics. The coupled semiconductors creates a built-in electrical field

at the interface due to their different Fermi levels, which can promote charge separation and accumulate the electrons and holes at different semiconductors. 3) Improving sample stability. Some effective photocatalysts usually suffer from the photocorrosion, which can be largely alleviated by coating a protect layer.

Although several heterojunctions are built based on their CB and VB positions of semiconductors, the most widely used configuration in photoelectrocatalysis is a type-II structure (Fig. 6a) [4]. Upon light absorption, the photogenerated electrons migrate from the semiconductor with a higher CB to that with a lower CB, while the photogenerated holes are accumulated at the semiconductor with the higher VB. The photocathode constructed upon this type-II structure is shown in Fig. 6b. Taking a two semiconductor heterojunction as an example, one (semiconductor A) with higher CB position generally interacts with a conductive substrate, while the other (semiconductor B) with lower CB position is coated on semiconductor A to form a heterojunction. Driven by built-in electrical field, the photogenerated electrons are accumulated at the CB of semiconductor B to carry out reduction reactions, while the holes are transported to the counter electrode. Given these advantages, the heterojunctions by semiconductor composites have made great achievements on constructing photocathodes for CO_2 reduction. Cu_2O, a typical p-type semiconductor, is regarded as an excellent candidate for PEC CO_2 reduction [104]. The formation of heterojunctions with other semiconductors has been extensively investigated. An attractive way is to integrate Cu_2O with CuO, as they can couple well at the interface [75,82,105]. Takanabe *et al.* [105] reported a Cu_2O/CuO heterojunction photocathode on Cu foil. Cu_2O film was firstly obtained by thermal oxidation of Cu foil, which significantly reduces interfacial resistance and suppresses charge recombination. Then CuO nanowires were formed on the surface of Cu_2O at higher oxidation temperature (Fig. 7a). The strong electric field at the interface facilitated charge separation and migration. After initial galvanostatical reduction, the photocathode based on Cu/Cu_2O/CuO nanowires showed a photocurrent of 1.67 mA cm^{-2} and 60% selectivity for CO_2 reduction at −0.6 V *versus* RHE (Fig. 7b).

In addition to Cu_2O, other Cu-based semiconductor heterojunctions also exhibit remarkable performance. For instance, a $CuFeO_2$/CuO mixed catalyst was synthesized through electroplating (Fig. 7c) [40]. Constructing a setup for CO_2 reduction, the $CuFeO_2$/CuO photocathode produced formate with over 90% selectivity under simulated

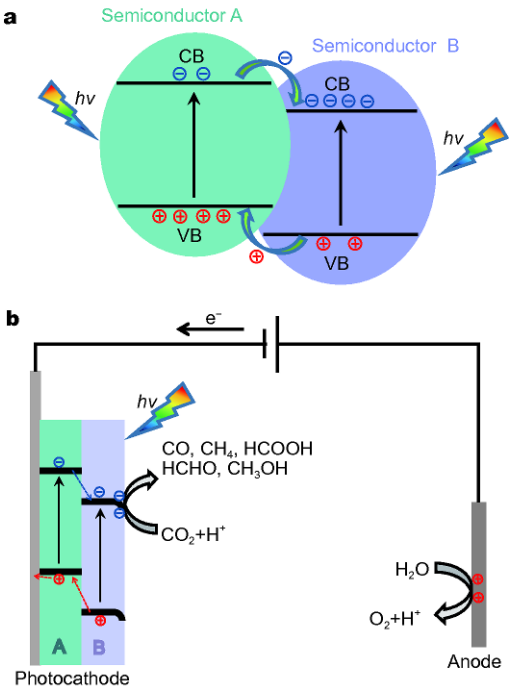

Figure 6 Schematic diagrams for (a) type-II structure heterojunction and (b) photocathode components.

solar light without any external electrical bias (Fig. 7d). The setup could maintain for over 1 week at a solar-to-formate energy conversion efficiency of ~1%. In parallel, ZnTe is a promising p-type semiconductor for CO_2 reduction owing to its narrow band gap (~2.26 eV) and negative CB position (−1.63 V *versus* RHE) [106]. Lee's group developed a ZnTe/ZnO nanowire heterojunction photocathode for CO_2 reduction, which exhibited outstanding PEC CO_2 conversion to CO [36,37].

Despite their widespread applications in PEC reduction reactions, the photocathodes by p-type semiconductors generally suffer from relatively low stability in aqueous solution, which largely limits further developments [20,25]. For CO_2 reduction, photocathode endures more serious challenges owing to the complicated reaction processes at surface. Coating with a protective heterojunction layer is an effective approach to mitigate the corrosion. In the design, two necessary factors for the heterojunction layer should firstly be taken into account: minimal band offset and high-quality interface [107]. The former can minimize the electron tunneling barrier to facilitate charge transport, while the later suppresses charge combination.

Several protective layers have been exploited for protecting photoelectrode. Silicide [108], TiO_2 [109] and

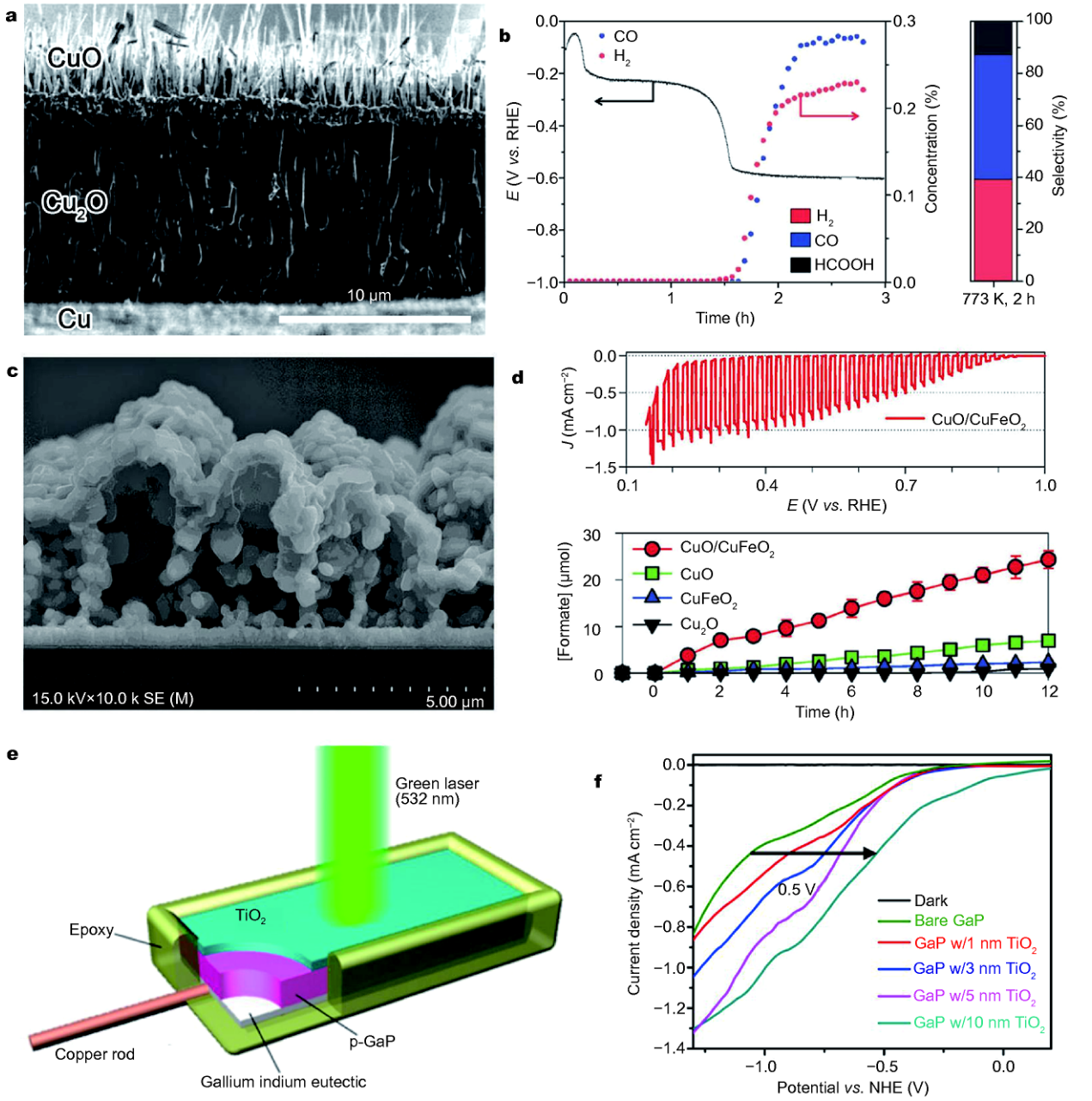

Figure 7 (a) SEM image and (b) Chrono potentiometric measurements at a constant current density of 1.67 mA cm^{-2} for Cu/Cu_2O/CuO nanowires photocathode. Reproduced with permission from Ref. [105]. Copyright 2014, the Royal Society of Chemistry. (c) SEM image of $CuFeO_2$/CuO mixed film. (d) Photocurrent response and PEC formate production for $CuFeO_2$/CuO mixed film. Reproduced with permission from Ref. [40]. Copyright 2015, the Royal Society of Chemistry. (e) Schematic diagram for the TiO_2 passivated p-GaP photocathode. (f) Photocatalytic current-potential curves of p-GaP photocathodes with different TiO_2 thicknesses. Adapted with permission from Ref. [38]. Copyright 2014, the American Chemical Society.

$SrTiO_3$ [22] have demonstrated their fascinating potential for improving stability in CO_2 reduction. For instance, the Al-doped ZnO/TiO_2 layer, which had been developed to serve as an effective protective layer for water reduction [21], was recently employed to protect Cu_2O photocathode for CO_2 reduction with the largely improved stability [33,110]. Moreover, a thin film of n-type TiO_2 was deposited on p-GaP by atomic layer deposition (ALD) to passivate the surface (Fig. 7e) [38]. The conformal deposition maximally eliminated the interface

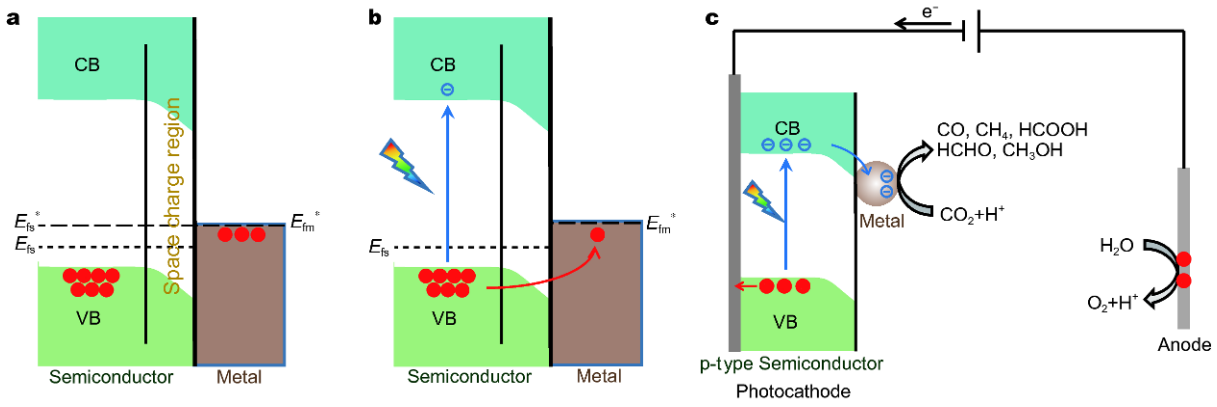

Figure 8 Schematic illustration for (a) the Schottky junction between metal and p-type semiconductor and (b) the charge migration in photocatalytic process. (c) Schematic illustration for the charge migration in the photocathode anchored with metal nanoparticles under light illumination.

defects, providing a substantial enhancement on the photoconversion efficiency. In addition to the passivation effect, the n-type TiO_2 layer created a p-n junction with p-GaP photocathode. The formed built-in field could further assist charge separation and reduce charge combination. Benefiting from the merits, the p-GaP photocathode passivated with 10 nm TiO_2 demonstrated a 0.5 V shift of onset overpotential for CO_2 reduction to CH_3OH (Fig. 7f). After 8 h of illumination by a green laser (532 nm), the photocathode produced 4.9 μmol of CH_3OH with FE of 55%.

Anchoring co-catalysts on photocathodes

The efficiency for CO_2 reduction is limited by the kinetic sluggishness of multi-electron-participating reactions that causes a large overpotential to overcome. In general, the CO_2 adsorption and activation are initial steps for subsequent reductions. For PEC CO_2 reduction, semiconductor photocathodes usually perform as both light-harvesting antennas and catalytic sites. Although numerous efforts have been put on improving light harvesting efficiency to supply sufficient electrons, semiconductor surface shows the frustrating ability for CO_2 adsorption and activation, resulting in the low efficiency and selectivity for CO_2 conversion [27,28]. It is generally believed that anchoring co-catalysts with high activity at semiconductor surface is an effective approach to improve the efficiency of CO_2 reduction, which has achieved glorious accomplishments in photocatalytic processes [19,111,112]. The co-catalysts can lower the overpotential and reduce the energy barrier, facilitating CO_2 activation. Meanwhile, reduction pathway can be specially designated by selecting specific co-catalysts, improving the selectivity of desirable products. Borrowing from those merits, co-catalysts are employed to improve the efficiency and selectivity of CO_2 reduction in PEC processes. In this section, we will outline the diversified co-catalysts which have been used for semiconductor photocathodes and discuss their mechanisms and fundamentals. Several representative achievements with co-catalysts are summarized in Table 3.

Metal nanoparticles

It is well recognized that hybridizing semiconductor with metal nanoparticles as co-catalysts is an effective strategy for boosting the performance of photocatalysis [111,113]. The metal co-catalysts play two positive roles in the photocatalysis: 1) trapping the photo-induced charges to promote charge separation; and 2) performing as catalytic active sites to lower the overpotential and carry out the reaction. In a photocatalytic process, directly anchoring metal nanoparticles on semiconductor can form the Schottky junction at the interface [4]. In a p-type semiconductor, the electrons on metal will flow to semiconductor after contact if the work function (W) of semiconductor is larger than that of metal (i.e., $W_s > W_m$). This electron flow bends downwards the energy band to form a space charge region as shown in Fig. 8a. The space charge region formed by the Schottky junction is dynamic. Upon light irradiation, the photogenerated holes of p-type semiconductor will firstly be accumulated on the VB due to the space charge region, which weakens the Schottky junction and breaks the dynamic equilibrium. When the accumulated holes can sufficiently compensate the electrons in the Schottky junction, the holes will transfer to the metal and the Schottky junction will be re-established to prevent the holes from flowing back. Eventually, the photogenerated holes will be accumulated

on the metal (Fig. 8b). As a result, it seems that metal nanoparticles anchored on p-type semiconductor cannot serve as active sites for the electron-participating reductions.

However, it behaves differently in a PEC system (Fig. 8c) [8]. As p-type semiconductor is the component of photocathode, the photogenerated holes will be separated and migrate toward the counter electrode with the assist of external electrical bias upon light illumination, triggering oxidation reactions (e.g., water oxidation). At the same time, the electrons will accumulate on the surface of photocathode. As such, if metal nanoparticles are anchored on the surface of photocathode, the electrons will flow to the metal and participate in reduction reactions (i.e., CO_2 reduction).

After the electrons are accumulated on the metal nanoparticles anchored on semiconductor photocathode, the reduction reactions will be carried out on the metal surface. Although various metals can serve as excellent co-catalysts for photocatalysis, not all metals are suitable candidates for CO_2 reduction [13]. The concern is derived from the major competitive reactions (i.e., hydrogen evolution reaction). As shown in Fig. 9, most metal materials serve as excellent catalysts for hydrogen evolution, especially for Pt. As a matter of fact, the dominated product would be hydrogen so as to largely suppress CO_2 reduction if Pt was employed as a co-catalyst [114]. Fortunately, some metals are competent to act as active sites for CO_2 reduction.

Generally speaking, Au [115], Ag [116] and Pd [117] facilitate the reduction to CO in CO_2-saturated aqueous electrolyte while Sn [118] and Pb [119] are beneficial to formate evolution. Notably, Cu can yield rich hydrocarbon products from CO_2 reduction, such as methanol and methane, which have received giant attention for both photocatalytic and electrocatalytic processes [120–122]. In terms of PEC CO_2 reduction, one should also consider those matters to improve the Faradaic efficiency and suppress the competitive reactions when employing metals as co-catalysts.

Many pioneering researches have investigated the effect on PEC CO_2 reduction after anchoring metal nanoparticles on photocathodes [69,123,124]. Although discrepant results were often obtained from the reported literature, which mainly resulted from different experimental methods and conditions, similar trends could be summarized. Anchoring metal nanoparticles could positively shift the overpotential of CO_2 reduction and modulate the types of products. For instance, p-Si photocathode was modified by small Cu, Ag and Au nanoparticles for PEC CO_2 reduction [123]. The light illumination induced more positive potential of ca. 0.5 V than that of corresponding metal electrodes. CO and HCOOH were main products for Ag and Au, while CH_4 and C_2H_4 were readily formed in the presence of Cu co-catalyst.

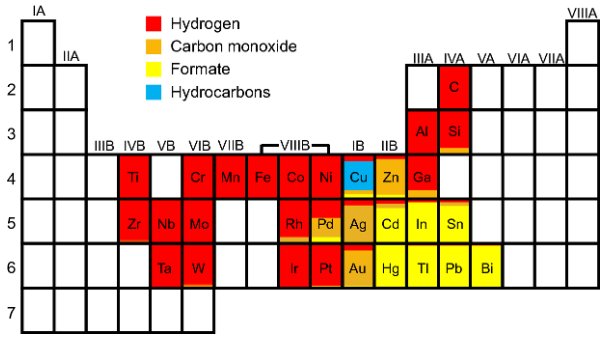

Figure 9 Periodic table depicting the primary reduction products from the reaction system of CO_2 and H_2O on metal and carbon electrodes. Adapted with permission from Ref. [13]. Copyright 2015, the American Chemical Society.

In another report, Kaneco *et al.* [69] deposited Pb, Ag, Au, Pd, Cu and Ni on p-InP photocathode as co-catalysts and systematically investigated their performance in PEC CO_2 reduction in LiOH/methanol electrolyte. The experimental results implied that Pb, Ag, Au and Cu produced both CO and HCOOH while CO was the only product for Pd. Although hydrocarbons (i.e., methane and ethylene) could be obtained from Ni-deposited photocathode, FE was quite low (0.7% and 0.2%, respectively). The distribution of reduction products for the metal–modified p-InP photocathodes were associated with the different enthalpy and Gibbs energy of dissociative adsorption of CO(g) on metal surface. Given the promising performance in CO_2 reduction, copper was particularly investigated as a co-catalyst on p-InP photocathode [125], which dominantly modulated the products of reduction. CH_4 and C_2H_4 were formed after the addition of Cu nanoparticles; otherwise, only CO and HCOOH were obtained.

Subtle designs for the nanostructures of photocathode materials can satisfy the demand for efficient light utilization, but still suffer from the absence of high active sites to trigger the activation and conversion of CO_2. On the basis of pioneering investigations, several achievements have recently been fulfilled to improve the efficiency of PEC CO_2 reduction by anchoring metal nanoparticles as co-catalysts on nanostructured photocathodes. Taking 1D p-Si nanowire arrays as an example, their efficiency was

a

	Charge[a] (C)	Formic acid (μmol h^{-1} cm^{-2})	F.E. (%)	Methanol (μmol h^{-1} cm^{-2})	F.E. (%)	CO (μmol h^{-1} cm^{-2})	F.E. (%)
Bare	0.93	0.231	4.78	0.024	1.49	0.250	5.64
Ag	0.72	0.368	9.81	0.015	1.23	0.272	7.25
Au	0.68	0.568	16.05	0.077	6.54	0.258	7.90
Cd	0.94	0.506	10.38	0.078	4.79	0.243	5.45
Cu	0.78	0.602	14.90	0.010	8.20	0.244	6.60
Pb	0.52	0.524	19.32	0.102	11.33	0.243	9.80
Sn	0.66	0.329	9.55	0.054	4.57	0.251	7.95

[a] Total charge used in CO_2 reduction reaction ($=\int I\,dt$; where I is the measured current and t is the reaction time) for 1 h in CO_2-bubbled 0.1 mol L^{-1} $KHCO_3$ aqueous solution at −0.4 V (*vs.* SCE).

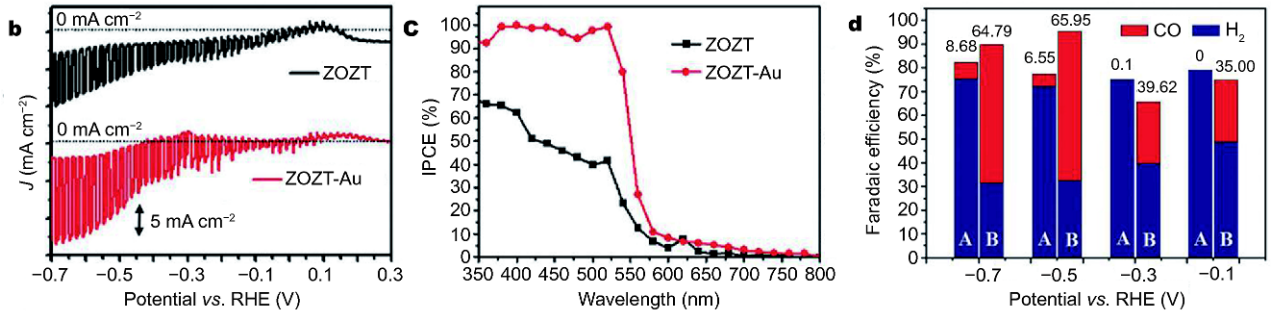

Figure 10 (a) The results of PEC CO_2 reduction with bare and metal-decorated CuO/Cu_2O films as photocathodes. Reprinted with permission from Ref. [75]. Copyright 2014, Elsevier. (b) Photocurrent response, (c) IPCE values and (d) FEs of CO and H_2 from the PEC CO_2 reduction with ZnTe/ZnO (A) and Au-coupled ZnTe/ZnO (B) photocathodes. Reproduced with permission from Ref. [36]. Copyright 2015, the Royal Society of Chemistry.

still low, although 1D configuration improved the evolution of products. However, after Sn nanoparticles were coupled to photocathode as a co-catalyst, the amount of formate production was enhanced by a factor of five along with an FE of 45.5%, and the competitive H_2 production was reduced by the addition of Sn (shown in Fig. 4c) [29]. In parallel, Woo *et al.* [75] deposited various metals on CuO/Cu_2O films and investigated their performance for PEC CO_2 reduction. The deposited transition metals effectively enhanced the CO_2 conversion to fuels in terms of Faradaic efficiency (Fig. 10a). In particular, Pb demonstrated outstanding performance among the transition metals: 0.524 μmol h^{-1} cm^{-2} for HCOOH, 0.102 μmol h^{-1} cm^{-2} for CH_3OH and 0.243 μmol h^{-1} cm^{-2} for CO with a total FE of 40.45% at 0.4 V *versus* SCE.

Overall, the rational selection of semiconductor and co-catalyst holds the promise for efficient CO_2 reduction. For instance, although ZnTe is an excellent candidate for CO_2 reduction due to its narrow band gap and negative CB position, the H_2 evolution was verified to be the dominant reaction at the surface of ZnTe during the PEC process, largely suppressing the reduction of CO_2. It was found that the use of Au nanoparticles as a co-catalyst was an effective approach to enhance the activity and selectivity of CO_2 conversion to CO [36]. As depicted in Fig. 10b–d, Au nanoparticles induced a larger photocurrent response (16 mA cm^{-2}) with an IPCE value of 97% at −0.7 V *versus* RHE. More importantly, the competitive water reduction was strongly suppressed while enhancing the FE of CO production from 7.2% to 58%. The remarkable improvement by Au co-catalyst originated from the formation of a Schottky junction with ZnTe that improved charge separation and the supply of reaction centers for CO_2 reduction.

Metal complexes

Apart from metal nanoparticles, homogeneous metal complexes are also attractive catalysts for CO_2 reduction [5,27,112]. The multiple and accessible redox states of metal complexes can facilitate the multi-electron reduction process of CO_2 [126]. Meanwhile, the redox potential of CO_2 can be modulated by tuning the configuration of complexes, which eventually alters the selectivity of products. Grafting the metal complex on photocatalyst as a co-catalyst is a promising approach to enhance the activity for CO_2 conversion. The photogenerated electrons can transfer to the metal complex, and become separated from holes to suppress the recombination. Then the electrons induce the reduction of metal centers to serve as active sites for the activation of adsorbed CO_2 molecules.

One essential requirement is that the lowest unoccupied molecular orbital (LUMO) of metal complex should be more positive than the CB position of semiconductor substrate to ensure the thermodynamically favorable transfer of electrons [5]. Glorious achievements have been fulfilled in the photocatalytic process that ex-

hibits high turnover number (TON) and selectivity for desirable products [127]. Re- and Ru-based complexes have been extensively investigated and commonly employed as co-catalysts. Some representative complexes, which demonstrate excellent performance for CO_2 conversion to CO, are structured in Fig. 11a–c. The proposed mechanism for CO production using $Re(bipy)(CO)_3X$ as a catalyst is depicted in Fig. 11d [128].

The applications of metal complexes in PEC CO_2 reduction have also been widely developed [112,129,130]. In 2010, Kubiak *et al.* [129] took $Re(bipy\text{-}Bu^t)(CO)_3Cl$ as a co-catalyst to enhance the activity of p-Si photocathode for CO_2 reduction to CO. Even though the metal complex was directly dissolved into electrolyte without chemical grafting to cathode, a giant enhancement was still achieved with a high FE of 97% for CO production. To facilitate the electron transfer, metal complex was intentionally grafted on the surface of photocathode. The linkage can prevent the shed of metal complex, improving the stability of photocathode during the reduction process [70,110,130].

Most recently, the covalent immobilization of Re-based complex on mesoporous TiO_2 modified Cu_2O photocathodes for CO_2 reduction to CO was reported (Fig. 12a) [33]. Taking acetonitrile as electrolyte, the designed photocathode boosted photocurrent density while sustaining high FE of 80–95% for 1.5 h. Ru-based complexes were also employed as co-catalysts for enhancing the activity and selectivity of PEC CO_2 reduction [34,45,131,132]. For instance, Zn-doped p-InP photocathode was modified by a Ru-complex polymer catalyst $[Ru(L\text{-}L)(CO)_2]_n$ [131]. After reaction for 3 h at −0.6 V *versus* Ag/AgCl under visible light illumination, formate was produced with a concentration of 0.17 mmol L^{-1} and FE of 62%, while no product was detected using the unmodified photocathode. In addition, a p-type sulfide semiconductor ($Cu_2ZnSn(S,Se)_4$, i.e., CZTSSe) with a narrow band gap was also modified by Ru complex [34]. The modified CZTSSe photocathode demonstrated a similar enhancement for CO_2 reduction, achieving 0.49 mmol L^{-1} of formate with an FE of 80% after 3 h reaction at −0.4 V *versus* Ag/AgCl under visible light.

It is worth mentioning that Ishitani group have recently developed a novel metal complex consisting of both Re and Ru elements [133]. The Ru(II)-Re(I) supramolecular metal complex exhibited superior performance for CO_2 reduction to Re and Ru single metal complexes. In this metal complex, Re center served as an active site for CO_2 reduction while Ru complex component could absorb visible light to sensitize photocathode. The integration of

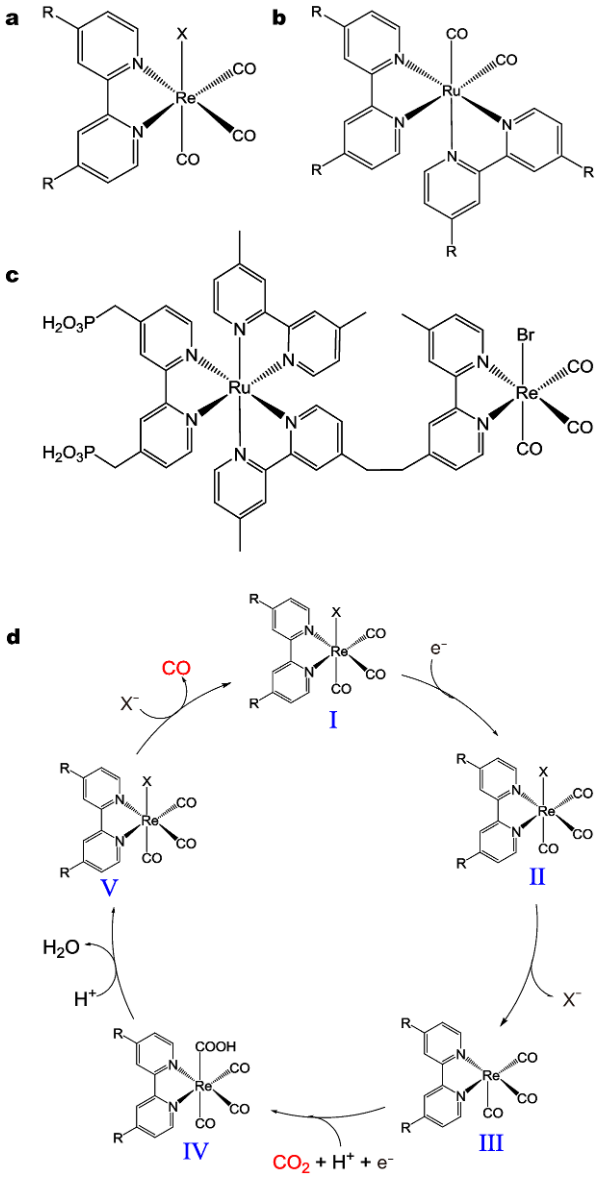

Figure 11 The molecular structures of (a) $Re(bipy)(CO)_3X$, (b) $[Ru(dcbpy)_2(CO)_2]^{2+}$ and (c) Ru(II)-Re(I) binuclear complex. (d) Proposed mechanism for CO_2 reduction to CO using $Re(bipy)(CO)_3X$ as a catalyst.

a p-type NiO cathode with this complex induced an intrinsic improvement for CO_2 reduction to CO (Fig. 12b) [134]. The TON reached 32 with FE of 62% after reacting for 3 h, and excellent durability was achieved when the reaction was prolonged to 5 h with FE increased to 98%.

Despite the remarkable performance in CO_2 conversion, typical metal complexes contain noble metal centers (e.g., Re and Ru), whose high costs impede their practical preparation and application. The development of low-cost transition metal complexes opens a bright window

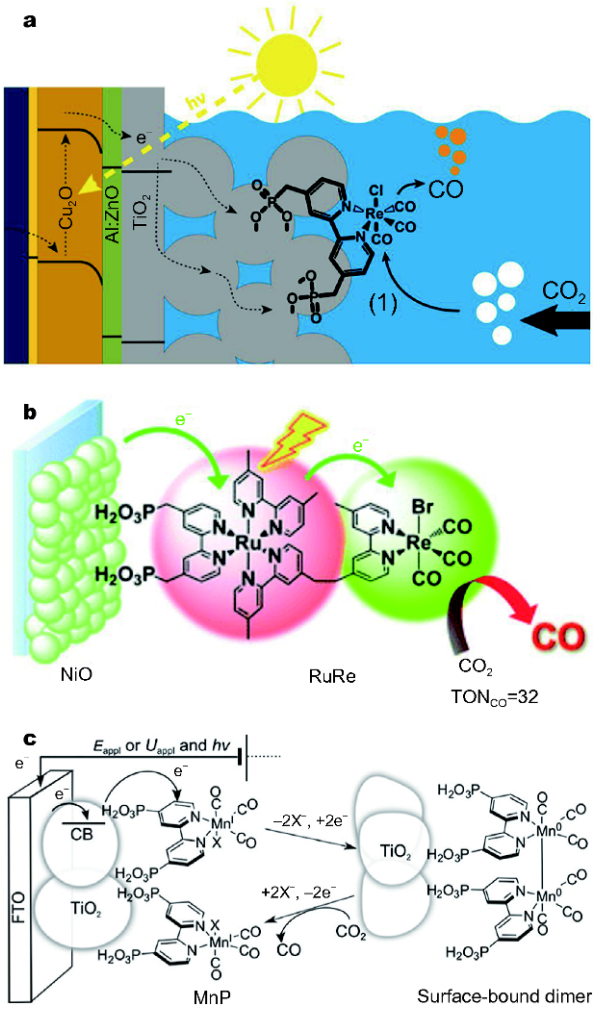

Figure 12 Schematic representations for (a) Re(bipy)$(CO)_3$Cl complex covalently bound to TiO_2-modified Cu_2O, (b) Ru(II)-Re(I) supramolecular modified NiO, and (c) molecular Mn catalyst-immobilized mesoporous TiO_2 photocathode for CO_2 reduction. Adapted with permission from Ref. [33], copyright 2016, the American Chemical Society, Ref. [134], copyright 2015, the Royal Society of Chemistry, and Ref. [140], copyright 2016, Wiley-VCH Verlag GmbH & Co, respectively.

for CO_2 reduction [127]. Several earth-abundant metals, such as Co [135], Ni [136], Mn [137] and Fe [138], are chosen to exploit active metal complexes, which have successfully been implemented in photocatalytic CO_2 reduction and demonstrated promising potential. Along this line, several advances have been achieved to enhance the performance for PEC CO_2 reduction by modifying photocathode with the non-noble metal complexes. In a typical case, a highly active Fe porphyrin complex was grafted on B-doped p-Si photocathode for CO_2 reduction [139]. The Fe porphyrin complex demonstrated a giant enhancement for CO evolution and efficiently suppressed competitive proton reduction, enabling a TON of 175 for CO production with FE of 80% after 6 h reaction. In parallel, a molecular manganese catalyst (*fac*-[MnBr(4,4'-*bis*(phosphonicacid)-2,2'-bipyridine)$(CO)_3$]) was immobilized on a mesoporous TiO_2 electrode (Fig. 12c) to achieve a TON of 112±17 with FE 67±5% of for PEC CO_2 reduction to CO after 2 h electrolysis [140]. Interestingly, this study revealed the dynamic formation of a catalytically active Mn-Mn dimer on the TiO_2 electrode surface.

Metal complexes have shown marvelous performance in catalytic CO_2 conversion; however, the two-electron reduction products (i.e., CO and HCOOH) are primarily formed, and higher-value hydrocarbon products (e.g., CH_3OH and CH_4) remain rare. Very recently, a trimethylammonio functionalized iron tetraphenylporphyrin complex was reported to trigger the eight-electron reduction of CO_2 to CH_4 under visible-light illumination [141]. With this complex combined with an Ir-based light sensitizer, CO was firstly obtained and then further reduced to CH_4 with a high selectivity of up to 82%. The remarkable catalytic performance achieved a quantum yield (light-to-product efficiency) of 0.18%. Based on this exciting finding, we outlook that the metal complex catalyst for CO_2 reduction to hydrocarbons can be employed for photoelectrocatalysis to achieve higher efficiency and produce higher-value products.

Organic molecules

Some organic molecules have been discovered to have a vital role on electrocatalytic CO_2 reduction [13,19]. In the reaction process, the organic molecules can participate in the reaction and perform as mediators to transfer electrons and protons to CO_2. In an early study, it revealed that tetraalkylammonium (NR_4^+, R=hydrocarbyl) salts dissolved in electrolyte could alter the catalytic properties of photocathode for CO_2 reduction. Bockris *et al.* [142] took a 0.1 mol L^{-1} solution of tetrabutylammonium perchlorate (TBAP) in DMF as electrolyte and p-type CdTe as photocathode to carry out CO_2 reduction, and obtained CO as the main product with a current efficiency of 70% at −1.6 V *versus* SCE. In addition, other tetraalkylammonium perchlorates could also promote the catalytic activity [143]. Mechanism investigations revealed that NR_4^+ ions have two effects on facilitating CO_2 reduction [144]: 1) the NR_4^+ ions adsorbed on photocathode can provide hydrophobic environment to impede the adsorption of H_2O and enhance the selectivity of CO_2 reduction; and 2) the NR_4^+ ions received electrons to form a $NR_4^{\bullet}$ radical intermediates, which served as a mediator to facilitate the activation of CO_2 to $CO_2^{\bullet-}$ (Equations 20,

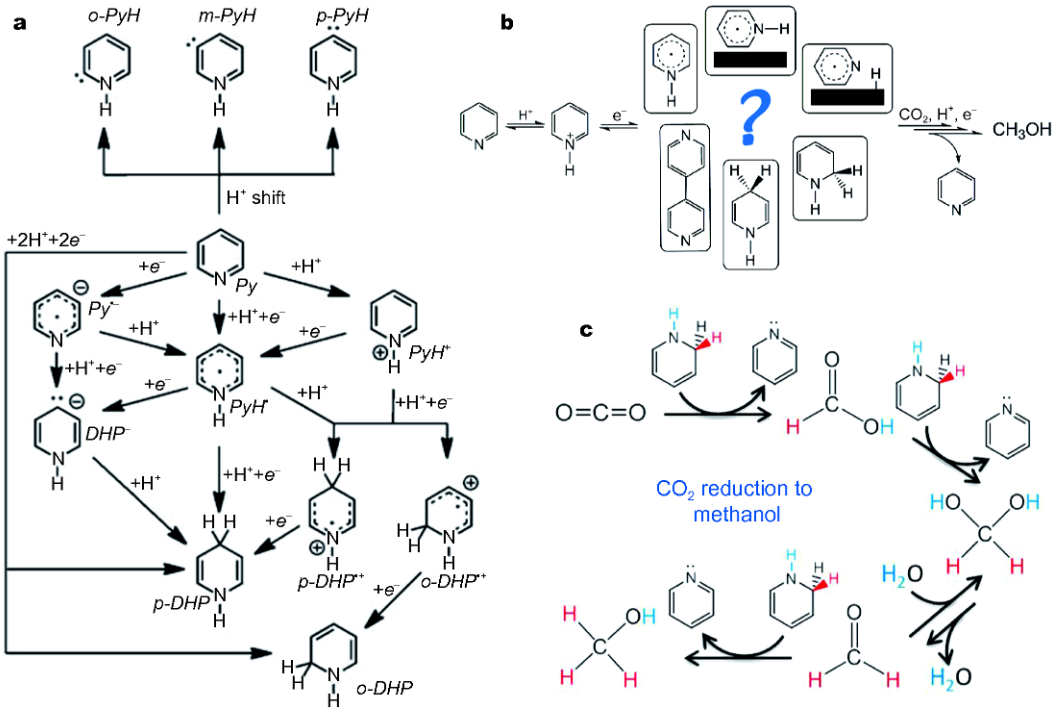

Figure 13 (a) Possible intermediates during the electrochemical reduction of pyridine. Adapted with permission from Ref. [147]. Copyright 2013, the Royal Society of Chemistry. (b) Some reported intermediates involved in the pathway of CO_2 reduction. (c) Reduction of CO_2 to methanol by a 1,2-dihydropyridine intermediate species *via* hydride and proton transfer steps. Adapted with permission from Ref. [153]. Copyright 2014, the American Chemical Society.

21).

$$NR_4^+ + e^- \rightarrow NR_4^{\bullet}, \quad (20)$$

$$CO_2 + NR_4^{\bullet} \rightarrow CO_2^{\bullet-} + NR_4^+, \quad (21)$$

Similarly in 2008, Bocarsly and co-workers reported that a protonated pyridine (i.e., pyridinium) molecule could serve as a remarkable co-catalyst when combined with p-GaP photocathode for CO_2 reduction [145]. The investigations on pH value indicated that pyridinium was an active catalyst while pyridine molecule alone could not. Notably the dominant product of CO_2 reduction was CH_3OH with a very high selectivity of 92% even at an applied potential lower than the standard redox potential for CO_2 to CH_3OH (−0.52 V *versus* SCE at pH 5.2). Since then, considerable attention has been paid on the pyridinium ion that serves as a cocatalyst for PEC CO_2 reduction. For instance, a p-$CuInS_2$ thin film photocathode together with pyridinium ions achieved the CH_3OH concentration of 1.2 mmol L^{-1} with FE of 97% after 11 h electrolysis at the overpotential of 20 mV [35]. A CdTe/FTO photocathode was also reported to have an enhancement on the PEC reduction of CO_2 to HCOOH [146].

Although it is well confirmed that pyridine molecules are firstly protonated to pyridinium ions and then participate in the process of CO_2 reduction as a mediator, the detailed mechanism for the pyridine-catalyzed CO_2 reduction is still ambiguous. The process may involve the complicated intermediates of pyridinium ions during reduction (Fig. 13a) [147]. Several research groups have hypothesized different reaction pathways through electrochemical experiments and theoretical calculations. Bocarsly's group proposed a one-electron shuttle model, in which pyridinium ion was firstly reduced to a pyridinyl radical and then combined with CO_2 molecule to form a pyridinyl radical-CO_2 complex [148]. This complex could be reduced to generate HCOOH and a cycled pyridine molecule. HCOOH could be further reduced to HCHO and then CH_3OH with pyridinyl radical.

However, Carter *et al.* [149,150] delivered the inconsistent results through theoretical calculations. The calculation for the redox potentials and acidity constants of pyridinium ions embodied two important results: 1) the redox potential of pyridinum to pyridinyl radical was −1.4 V *versus* SCE at pH 5.3, indicating a thermo-

dynamically unfavorable process with a high overpotential; 2) the pK_a of the pyridinyl radical was calculated to be as high as 27, suggesting that the deprotonations can hardly take place so that the formation of pyridinyl radical-CO_2 complex was disfavored. On this account, some other hypotheses were put forward to unravel the pathway of pyridine-catalyzed CO_2 reduction, including the surface adsorption of pyridinyl radical [149], the generation of surface hydride [151], the formation of carbamate radical by utilizing the bridged water molecules [152], the formation of 4,4'-bipyridine by coupling two pyridinyl radicals [147], and the multi-electron reduction to dihydropyridine intermediate [153] as depicted in Fig. 13b. For the moment, the formation of dihydropyridine intermediate seems more convictive than others based on the investigation evidences, which was kinetically and thermodynamically feasible in electron and proton transfers to CO_2 [150,153]. In this pathway, both HCOOH and HCHO could act as intermediate products and be further reduced to ultimately form CH_3OH (Fig. 13c). This mechanism has recently reported to be competent for PEC process [39].

Although it was declared that CH_3OH was the dominant product in the presence of pyridine molecules for CO_2 reduction, a very recent study found that CH_3OH could not be formed on preparative-scale and cyclic voltammetry bases. Detail characterizations revealed that CO_2 would merely indirectly participate in H_2 evolution *via* proton reduction in the presence of pyridinium ions and the formed Pt−CO film prevented the further reaction process [154]. The inconsistent result further indicated the complication of CO_2 reduction using pyridine as a co-catalyst.

Conductive polymers

Some conductive polymers, such as polyaniline [155], polypyrrole [156] and polydopamine [157], have been identified as component candidates for CO_2 reduction with lower overpotentials, especially in electrocatalytic processes. The polymers contain abundant functional groups, which can efficiently be bonded with reaction molecules and alter adsorption configurations. For instance, a recent study demonstrated that the polydopamine whose amine and hydroxylcarbonyl groups interacted *via* hydrogen bonds could feature a nucleophilic sequence and facilitate CO_2 binding [157]. Moreover, subtle control over the function groups of polymers can maneuver the formation of adsorbed hydrogen atoms (H_{ad}) and suppress the competitive hydrogen evolution, which in turn facilitates the hydrogenation of CO_2 and improves the selectivity of desirable products [155]. In this sense, it is an attractive strategy to enhance the performance of photocathodes in CO_2 reduction through the modification of conductive polymers as co-catalysts. The photogenerated electrons in photocathode can transfer to polymer and then participate in CO_2 reduction. In addition, it is feasible to *in situ* synthesize the polymer on photocathode through the polymerization of monomers, which can form perfect interface to avoid the trap and consumption of electrons.

The conductive polymers have demonstrated the potential in PEC CO_2 reduction as cocatalysts. Recently, a polypyrrole film was coated on p-CdTe (PPy/CdTe) photocathode by Woo *et al.* to enhance the catalytic performance [158]. The PPy/CdTe photocathode showed a prominent performance with an FE of 51% at −0.2 V *versus* RHE, whose production rates of HCOOH and CO are twice those of bare ZnTe electrode. Mechanism investigations revealed that the different work functions induced the facile electron transfer from ZnTe to PPy, suppressing charge recombination. Meanwhile, the PPy film supplied more active sites for CO_2 reduction, improving the FE of HCOOH and CO production.

The polycations (i.e., poly diallyldimethylammonium (PDDA) and poly(2-trimethylammonium)ethyl methacrylate (PMAEMA)) have also been explored for CO_2 reduction through integration with CdTe quantum dots (QDs) on ITO electrode by a directed layer-by-layer assembly method [159]. It was found that the structure of polycation and the assembly with QDs had a significant impact on the PEC performance. PMAEMA/QDs exhibited an enhanced activity under light illumination, while PDDA showed a negative effect on photo–induced reduction. On the other hand, the polycations determined the types of products. The products obtained with the PDDA/QDs assembly were CO, HCHO, CH_3OH and H_2, while only HCHO was detected as a product for PMAEMA/QDs electrode.

Enzymatic biocatalysts

Some redox enzymatic biocatalysts exhibit the fascinating talents for CO_2 reduction, and have been extensively investigated in both photocatalytic [160] and electrocatalytic [161] processes. The enzymatic biocatalysts typically show extremely high activity and selectivity for specific products without side reactions [162]. Anchoring the enzymatic biocatalyst on photocathode as a co-catalyst can supply highly active sites for CO_2 reduction, which dramatically boosts the activity and improves the selectivity. Karkinson *et al.* [163] firstly modified a p-InP

photocathode with a formate dehydrogenase (FDH) in early 1984. Although the denaturation of the protein led to activity loss, a current efficiency of 80%–93% for formate conversion with a TON of up to 21,000 at +0.05 V *versus* NHE was still achieved, demonstrating the great potential.

Recently, Armstrong's group have exploited highly active carbon monoxide dehydrogenase (CODH) to serve as the co-catalyst for PEC CO_2 reduction [32,164]. For instance, a CODH-form carboxydothermus hydrogenoformans was employed to functionalize a dye-sensitized p-NiO photocathode, which could selectively reduce CO_2 to CO under visible-light illumination with good stability (Fig. 14a) [32]. However, an expensive nicotinamide cofactor (NADH) is generally required to achieve catalytic turnover in such a biocatalytic process, and the regeneration of NADH usually limits the entire reaction. To solve this problem, Park *et al.* [165] designed an integrated enzyme-cascade (TPIEC) system using a Rh complex and three dehydrogenase (i.e., FDH, formaldehyde dehydrogenase (FaldDH), and alcohol dehydrogenase (ADH)), as depicted in Fig. 14b. NADH was consumed by dehydrogenases to generate NAD^+ during the reduction process, and then NAD^+ was catalytically reduced to NADH by Rh complex and electrons, fulfilling the regeneration with high efficiency. As a result, a high CH_3OH evolution rate of 1280 μmol h^{-1} g_{cat}^{-1} was achieved.

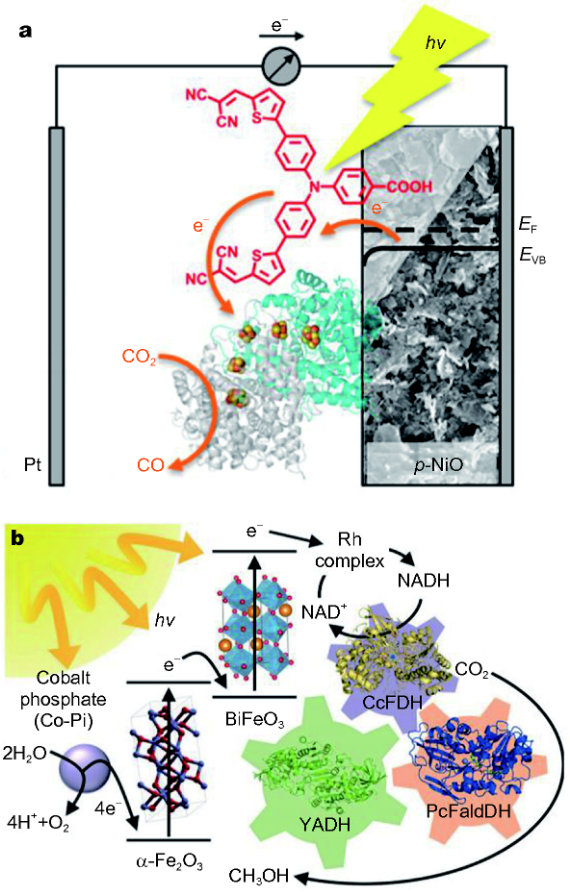

Figure 14 Schematic illustration for (a) a CODH functionalized dye-sensitized p-NiO photocathode for selective CO_2 reduction to CO and (b) a PEC enzyme-cascade system containing a Rh complex and three dehydrogenases for CO_2 reduction to CH_3OH. Adapted with permission from Ref. [32], copyright 2014, the American Chemical Society, and Ref. [165], copyright 2017, Wiley-VCH Verlag GmbH & Co, respectively.

OTHER SETUPS FOR PEC CO_2 REDUCTION

Combining photoanodes with dark cathodes

The development of photocathodes for CO_2 reduction has witnessed splendid achievements. However, giant challenges still exist and hinder the further improvement of conversion efficiency and selectivity. Commonly, the catalytic setups integrate light harvesting, charge separation and migration and CO_2 reduction processes on photocathode. The anode only serves as sites for water oxidation, which causes several disadvantages: 1) p-type semiconductors usually possess poor stability and are easily photocorroded under light illumination; 2) the VB positions of these semiconductors are not positive enough to trigger water oxidation, which requires a large external electrical bias; 3) semiconductors often do not offer highly active sites for catalysis. Although the anchored co-catalysts can improve the catalytic performance, the other issues have been hardly solved.

In comparison with p-type semiconductors, n-type semiconductors are much more exploited as light-harvesting antennas [10]. Many n-type semiconductors are earth-abundant and intrinsically stable, especially for metal oxides [166]. In general, photoanodes are fabricated by n-type semiconductors and applied to water oxidation [25,167]. Thus it is an alternative approach to employ a photoanode to harvest light with an effective cathode for CO_2 reduction, as depicted in Fig. 1b. In this PEC setup, the optimization of light harvesting and the engineering of catalytic sites are separated at anode and cathode, respectively, giving several merits [13]. Firstly, n-type semiconductors are better candidates for light utilization owing to their abundance and excellent stability. Secondly, after decoupled from light-harvesting component, the catalytic sites for CO_2 reduction can be engineered more flexibly by choosing and designing cathode mate-

Table 4 Selected recently reported PEC setups for CO_2 reduction

Electrode	Condition	Main products	Efficiency	Ref.
Combining photoanodes with dark cathodes				
Photoanode: Pt modified TNTs Cathode: Pt modified rGO on Ni foam	Anolyte: NaCl (1 mol L^{-1}), catholyte: $NaHCO_3$ (1 mol L^{-1}), constant potential: 2 V, Xe lamp (10 mW cm^{-2}), 8 h	CH_3OH, C_2H_5OH, HCOOH, CH_3OOH	1.13 μmol h^{-1} cm^{-2}	[169]
Photoanode: Pt modified TNTs Cathode: Pt modified rGO on Ni foam	Anolyte: NaCl (1 mol L^{-1}), catholyte: $NaHCO_3$ (1 mol L^{-1}), constant potential: 2 V, Xe lamp (10 mW cm^{-2}), 24 h	CH_3OH, C_2H_5OH, HCOOH, CH_3OOH	1.5 μmol h^{-1} cm^{-2}	[170]
Photoanode: Pt modified TNTs Cathode: Pt modified rGO on Cu foam	Anolyte: H_2SO_4 (0.5 mol L^{-1}), catholyte: $NaHCO_3$ (0.5 mol L^{-1}), constant potential: 2 V, Xe lamp	CH_3OH, C_2H_5OH, HCOOH, CH_3OOH	4.34 μmol h^{-1} cm^{-2}	[171]
Photoanode: TiO_2 nanorods Cathode: Cu_2O on Cu substrate	$KHCO_3$ (0.1 mol L^{-1}), 0.75 V *vs.* RHE, AM 1.5G light (100 mW cm^{-2}), 3 h	CH_4, CO, CH_3OH	FE: 54.63% FE: 30.03% FE: 2.79%	[31]
Photoanode: WO_3 film Cathode: glassy carbon type Cu	CO_2-purged $KHCO_3$ (0.5 mol L^{-1}, pH 7.5), 0.75 V *vs.* RHE, >420 nm (100 mW cm^{-2}), 1 h	CH_4	FE: 67%	[44]
Photoanode: WO_3 film Cathode: Sn/SnO_x	CO_2-purged KCl (0.5 mol L^{-1}, pH 5.2), 0.8 V *vs.* RHE, >420 nm (100 mW cm^{-2}), 3 h	HCOOH, CO	FE: 26.8% FE: 17.5%	[44]
Photoanode: Ni coated n-type Si Cathode: nanoporous Ag film	CO_2-saturated Na_2SO_4 (0.5 mol L^{-1}), external bias: 2V >400 nm, 3 h	CO	10 mA cm^{-2}, FE: 70%	[43]
Combining photoanodes with photocathodes				
Photoanode: p-Si nanowires Photocathode: n-TiO_2 nanotube arrays	CO_2-saturated $NaHCO_3$ (1 mol L^{-1}), −1.5 V *vs.* Ag/AgCl, AM 1.5G light, 30 min	CO, CH_4, C_2–C_4 products	824 nmol L^{-1} h^{-1} cm^{-2} 201.5 nmol L^{-1} h^{-1} cm^{-2}	[30]
Photoanode: Pt loaded TiO_2 Photocathode: p-type InP/Ru complex	$NaHCO_3$ (0.01 mol L^{-1}), no external applied electrical bias, AM 1.5G light, 24 h	Formate	TON: >17, FE: >70% SFE: 0.03–0.04%	[45]
Photoanode: CoO_x/TaON Photocathode: Ru(II)-Re(I) complex-p-NiO	CO_2-saturated $NaHCO_3$ (0.05 mol L^{-1}, pH 6.6), external electrical bias: 0.3 V, >400 nm, 1 h	CO	79 nmol, TON_{co}: 17, FE: 37%	[46]
Photovoltaic–based tandem electrocatalytic devices				
Photovoltaics: $CH_3NH_3PbI_3$ perovskite solar cell Anode: oxidized Au film Cathode: IrO_2	CO_2-saturated $NaHCO_3$ (0.5 mol L^{-1}, pH 7.2), supplied bias by photovoltaics: 2 V, AM 1.5G light (100 mW cm^{-2}), 18 h	CO	SCOE: 6.5% FE: 80–90%	[47]
Photovoltaics: GaInP/GaInAs/Ge solar cell Anode: SnO_2 modified CuO nanowires Cathode: SnO_2 modified CuO nanowires	Anolyte: CsOH (0.25 mol L^{-1}), Catholyte: $CsHCO_3$ (0.1 mol L^{-1}), supplied bias by photovoltaics: 2.24 V, AM 1.5G light (100 mW cm^{-2}), 5 h	CO	SCOE: 13.4% FE: 81% on average	[48]
Photovoltaics: Si based solar cells Photoanode: Co-Pi/W:$BiVO_4$ Photocathode: Pd/NR_x@TiO_2	CO_2-saturated $KHCO_3$ (0.1 mol L^{-1}), supplied bias by photovoltaics: 0.6 V by 5 W LED light, Xe lamp (200 mW cm^{-2}) for photoelectrode	CH_3OH	106 μmol L^{-1} h^{-1} cm^{-2} AQY: 95%	[187]
Wireless monolithic devices				
p-InP/[RuCP] + r-STO	H_3PO_4 buffered $NaHCO_3$ (0.1 mol L^{-1} pH 7.7), AM 1.5G light, no external applied electrical bias, 3 h	Formate	0.94 μmol, SFE: 0.08%	[132]
IrO_x/SiGe-jn/CC/p-RuCP	H_3PO_4 buffered $NaHCO_3$ (0.1 mol L^{-1} pH 7.7), AM 1.5G light, no external applied electrical bias, 2 h	Formate	50.2 μmol, SFE: 4.6%	[190]

rials.

Several research groups have successfully exploited this setup for PEC CO_2 reduction, as summarized in Table 4. As TiO_2 is a typical n-type semiconductor and considered as one of the most promising candidates for photocatalysis [168], the photoanodes based on TiO_2 were extensively employed to harvest light and combined with dark cathode to investigate the performance in CO_2 reduction. Cheng *et al.* [169] employed Pt modified TiO_2 nanotubes (Pt-TNT) as photoanode and Pt modified reduced graphene oxide (Pt-RGO) on Ni foam as dark cathode for PEC CO_2 reduction (Fig. 15a). The photogenerated electrons transferred from the photoanode to an external circuit and reached the cathode with the assist of a constant potential at 2 V. CO_2 was converted into several liquid products, including CH_3OH, C_2H_5OH,

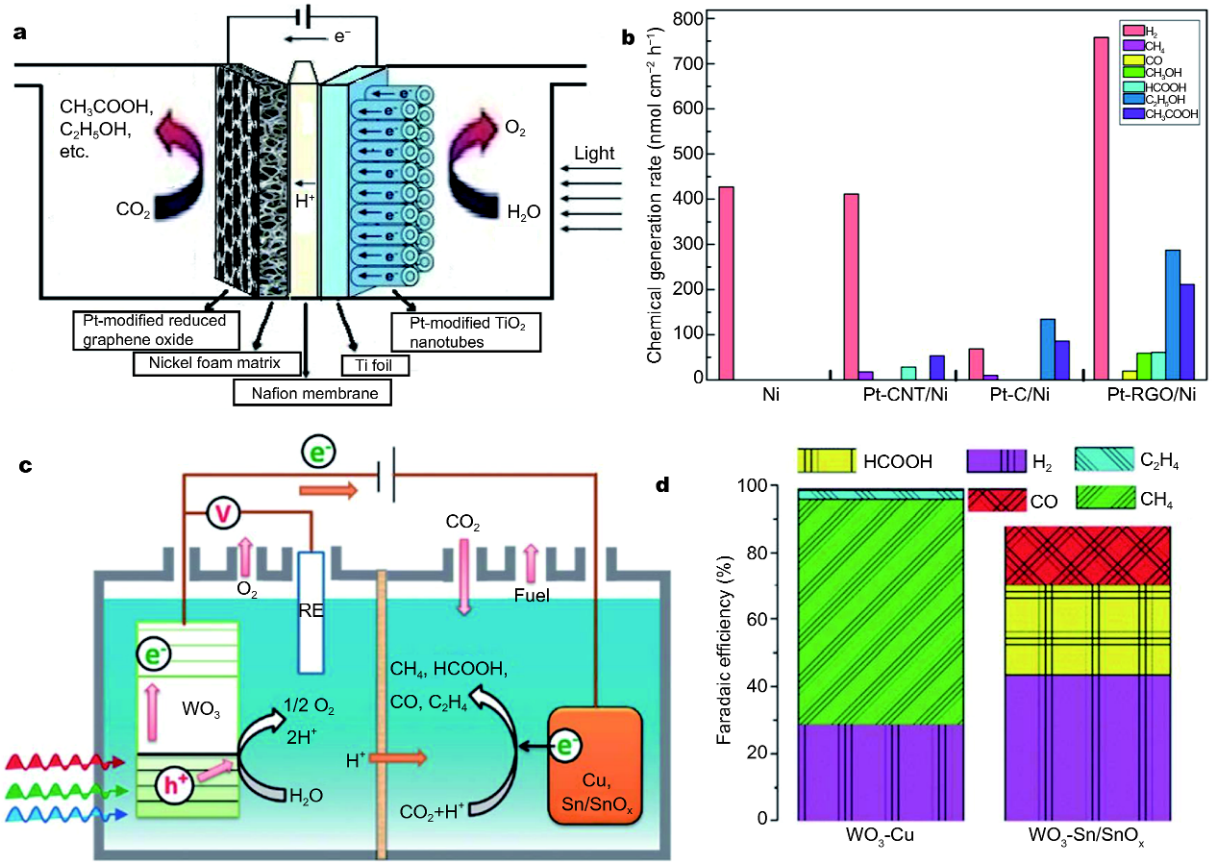

Figure 15 (a) Schematic diagram and (b) chemical generation rates of various products for the PEC setup that combines Pt-modified TiO_2 nanotubes as photoanode and Pt-modified rGO as dark cathode for CO_2 reduction. Adapted with permission from Ref. [169]. Copyright 2014, the American Chemical Society. (c) Schematic representation and (d) product distribution for the PEC system of CO_2 reduction that utilizes a WO_3 photoanode and Cu or Sn/SnO_x cathode under visible-light irradiation. Adapted with permission from Ref. [44]. Copyright 2014, the Royal Society of Chemistry.

HCOOH, and CH_3COOH. The conversion rate of carbon atoms reached 1.13 μmol h^{-1} cm^{-2} (Fig. 15b). The optimization of Pt-RGO cathode induced an arresting enhancement of carbon atom conversion rate to 1.5 μmol h^{-1} cm^{-2} [170]. Replacing Ni foam with Cu foam as cathode substrate could further enhance the carbon atom conversion rate to 4.34 μmol h^{-1} cm^{-2} [171].

In addition to metal/carbon cathodes, some semiconductors have emerged as promising cathode materials for CO_2 reduction. Cu_2O is a typical case owing to its low toxicity, high abundance and excellent activity, which has been widely exploited as photocathode for CO_2 reduction [33,82,83]. However, the poor stability caused by photocorrosion hinders the further development of Cu_2O cathode [33]. To suppress the photocorrosion, Gong *et al.* [31] employed Cu_2O as a dark cathode, combined with a TiO_2 photoanode for harvesting light. This strategy largely alleviated the instability of Cu_2O, and achieved CH_4, CO and CH_3OH as main products with total FE of 87.4% and a selectivity of 92.6% for carbonaceous products.

In terms of photoanodes, other metal oxides were employed as the component of photoanodes for light harvesting. For instance, a WO_3 photoanode was used to harvest light, together with an efficient electrocatalyst as cathode (Fig. 15c) [44]. Cu cathode obtained CH_4 as the main product with an FE of 67% at 0.75 V *versus* RHE, while another Sn/SnO_x cathode could achieve a combined FE of 44.3% for HCOOH and CO at 0.8 V *versus* RHE (Fig. 15d). In addition to metal oxides, a Ni-coated n-type Si was also chosen as photoanode to construct a PEC setup with a nanoporous Ag cathode for CO_2 reduction to CO [43]. At an external bias of 2.0 V, the setup delivered a current density of 10 mA cm^{-2} with an FE of ~70%, and stabilized the performance up to 3 h.

In the configuration of integrating photoanode and dark cathode, photoanode serves as a light-harvesting

center and water oxidation takes place on its surface. The function of photoanode is the same as the component of PEC oxygen evolution device. As such, the strategies for improving the light utilization (e.g., light harvesting, charge separation and migration) can borrow from those for PEC water splitting, which have been perspicuously summarized by some recent reviews [8,9,20,25]. More importantly, the cathode plays a crucial role in determining the products of CO_2 reduction, especially for selectivity of the desirable products, which has been well corroborated by the case enumerated above (i.e., WO_3 photoanode with Cu or Sn/SnO_2 cathode).

Generally speaking, the excellent electrocatalytic materials for CO_2 reduction can perfectly perform as the cathode for PEC setup. Metal materials are typically regarded as robust electrocatalysts for CO_2 reduction owing to their low overpotentials and high activities [42]. We have emphatically outlined the broad prospect for metal materials as the co-catalysts of photocathode. Directly constructing the dark cathode with metal materials can also inherit those merits for CO_2 reduction. As different metal elements can offer specific selectivity for various products (e.g., Au for CO and Cu for hydrocarbons), one can rationally select one or more metal elements to construct cathode for the desirable products.

Apart from element types, other factors such as structure, morphology, size and composition can also intrinsically alter the reduction products. Recently, those factors have been extensively maneuvered to modulate the performance in electrocatalytic CO_2 reduction [172–175]. Due to the theme and length limitation of this review, we will not deeply discuss these matters in this review. One might stimulate inspirations through some recent reviews about electrocatalytic CO_2 reduction [42,50,176]. What we attempt to emphasize is that the extensively exploited metal electrocatalysts could be employed to construct the dark cathode for PEC CO_2 reduction, which offers the capability of boosting overall performance.

In spite of the promising potential for CO_2 reduction, two major limitations are intrinsically accompanied with the use of metal cathode, impeding the further development. One is the preciousness of noble metal, and the other is the simultaneous promotion of competitive water reduction. Recently, a large amount of novel materials have been studied in electrocatalytic CO_2 reduction, including transition metal oxides [177,178], chalcogenides [179,180], and carbon-based materials [181,182]. These candidates are derived from earth–abundant elements and bypass the predicament of noble metals. Moreover, the special surface configurations endow high Faradaic efficiency for CO_2 reduction through the efficient adsorption and activation of CO_2 molecules, which steers the reaction pathway and suppresses competitive water reduction. Although the application of these materials has rarely been reported for PEC setups, we highlight that they would boost extraordinary talents in the future. Given their semiconducting properties, anchoring the materials on photocathode might be an alternative strategy for improving the catalytic performance in CO_2 reduction, which could both steer charge kinetics and serve as excellent co-catalysts.

Combining photoanodes with photocathodes

For a single-junction setup, photocathode or photoanode generally serves as a light-harvesting antenna for the conversion of solar energy to chemical energy. To optimize the light utilization, semiconductors are designed to extend light absorption, which typically needs to narrow the bandgap [4]. However, limited by the thermodynamic requirement for CO_2 reduction and water oxidation, the semiconductor with a narrow band gap cannot supply energetic electrons/holes to trigger the reduction/oxidation reactions [15,17]. Although this matter also limits water splitting, the situation should be more severe for CO_2 reduction as it commonly suffers from large overpotential. As a result, the modulation of band gaps for CO_2 reduction is caught in a dilemma. Although an external electrical bias can be applied to alleviate this predicament in a PEC process, it would be highly desirable to construct the PEC setup for CO_2 reduction for minimal applied external electrical bias toward sustainable production.

Natural photosynthesis provides an elegant strategy for converting CO_2 to carbohydrates, which has successfully inspired researchers to exploit a Z-scheme photocatalytic system to fulfill water splitting and CO_2 reduction [183,184]. On this account, the combination of photoanode with photocathode supplies a prospective approach to CO_2 reduction with minimal external electrical bias (Fig. 1c) [28]. In this setup, a n-type semiconductor with sufficiently positive VB position for water oxidation and a p-type semiconductor with sufficiently negative CB position for CO_2 reduction are employed as photoanode and photocathode, respectively. The semiconductor with a narrow band gap can be also suitable for this setup, achieving the maximization of light absorption (depicted in Fig. 16a).

Several subtle advances have been reported to achieve CO_2 reduction with high efficiency and minimal external

electrical bias (Table 4). A pioneering work was the PEC cell reported by Grimes *et al.* [30] using p-Si nanowires and n-TiO_2 nanotube arrays as electrodes. Although hydrogen evolution was still predominant, this setup obtained CO as the main product of CO_2 reduction under light illumination with a production rate of 824 nmol L^{-1} h^{-1} cm^{-2} at −1.5 V *versus* Ag/AgCl. In the meantime, CH_4 and trace of C_2-C_4 hydrocarbons with a combined rate of 201.5 nmol L^{-1} h^{-1} cm^{-2} were simultaneously evolved. In order to improve the efficiency and selectivity, versatile strategies were taken to optimize photoelectrodes, especially for photocathode. In a typical case, a Ru-based complex was anchored on p-InP photocathode while Pt-loaded TiO_2 served as photoanode for water oxidation [45]. Although the competitive water reduction cannot be completely eliminated, the FE for formate could achieve more than 70% with TON>17 at 24 h without external electrical bias. However, the solar-to-fuel efficiency (SFE, i.e., 0.03%–0.04%) was still low. In parallel, another metal complex (Ru(II)-Re(I) supramolecular metal complex) was also selected to modify a p-NiO photocathode [46]. As shown in Fig. 16b, the Ru(II) center could sensitize photocathode for enhanced light absorption, and the electrons transferred to the Re-based complex that worked as active sites for CO_2 reduction. It was verified that the absence of metal complex induced a negligible activity for CO_2 reduction. Combined with a CoO_x/TaON photoanode, the PEC cell enabled visible-light-driven CO_2 reduction by using water as a reductant to generate CO and O_2 with an external electrical bias of 0.3 V.

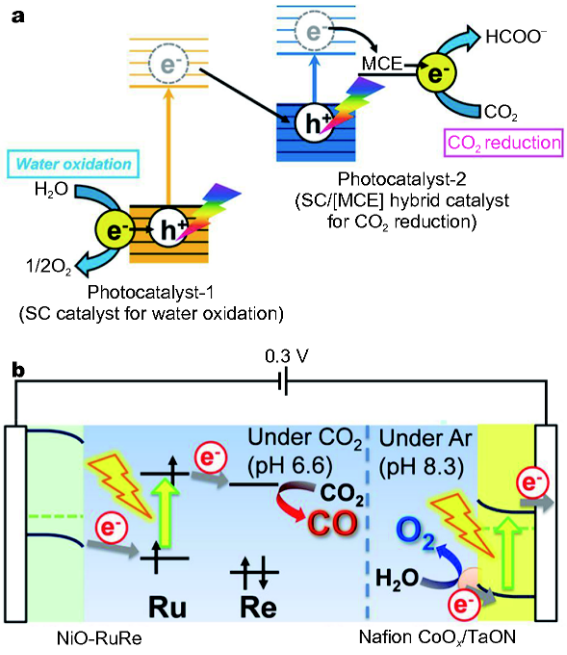

Figure 16 (a) Schematic illustrating the Z-scheme system for CO_2 reduction. Adapted with permission from Ref. [45]. Copyright 2011, the American Chemical Society. (b) Schematic illustration for the PEC setup with Z-scheme configuration consisting of Ru(II)-Re(I) metal complex modified p-NiO photocathode and CoO_x/TaON photoanode for CO_2 reduction to CO. Reproduced with permission from Ref. [46]. Copyright 2016, the American Chemical Society.

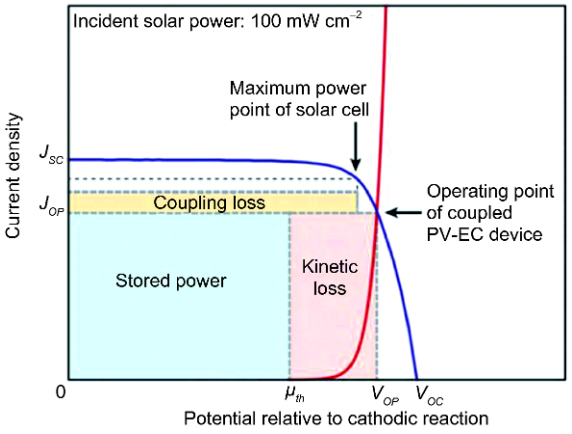

Figure 17 The generalized current density-voltage (*J*-*V*) diagram of a directly coupled photovoltaic-electrochemical device graphically which identifies the power flows relative to total incident solar power. Adapted with permission from Ref. [185]. Copyright 2013, the National Academy of Sciences.

Photovoltaic–based tandem electrocatalytic devices

Another alternative strategy for alleviating the dilemma between extending light absorption and matching redox potentials is to construct a tandem device [13], which connects a photovoltaic cell with an efficient electrolyzer for CO_2 reduction, as described in Fig. 1d. The photovoltaic cell can well match the solar spectrum to maximize light utilization, inducing high incident photon-to-electron conversion efficiency (IPCE) to supply sufficient electrical current for the reactions. Meanwhile, the robust voltage can also be provided by series-connecting photovoltaic cells to satisfy the thermodynamic redox potentials of CO_2 reduction and water oxidation. This concept has been well performed in water splitting, achieving high solar-to-hydrogen efficiency [185,186]. Notably, the basic principle for constructing this tandem device is that the operating point of electrolysis system must be as much as close to the maximum power point of photovoltaic cell, in order to minimize the energy loss in converting electrical energy to chemical energy (Fig. 17) [185].

Since the successful achievement for water splitting, Grätzel and co-workers employed perovskite photo-

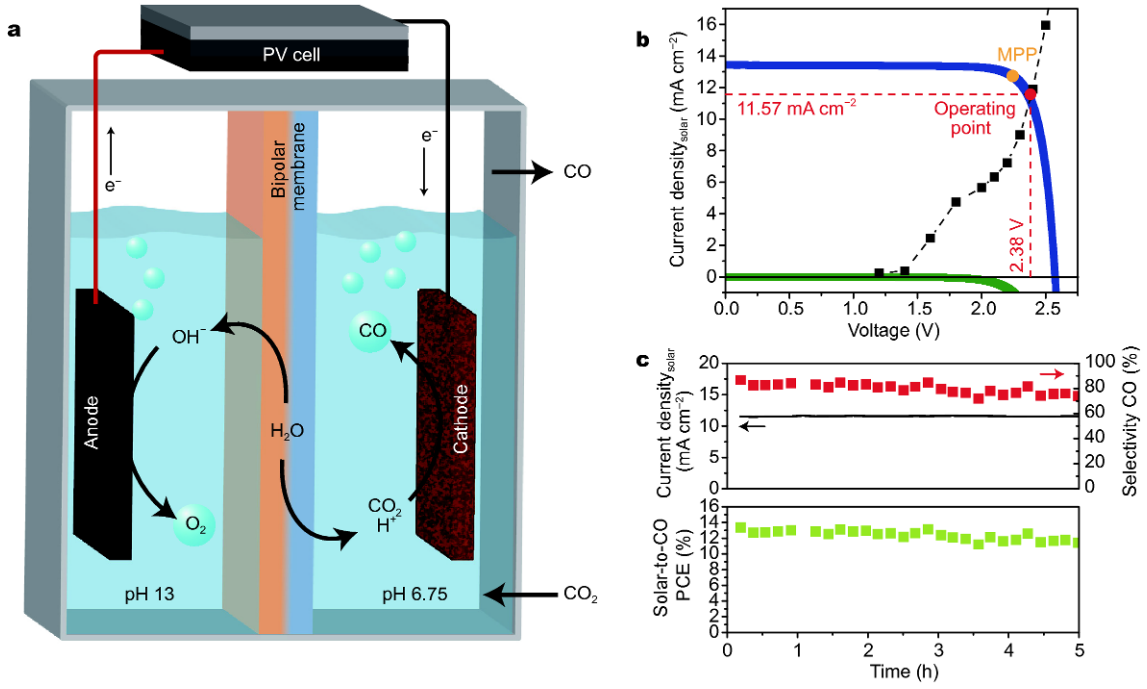

Figure 18 (a) Schematic illustration for the solar-driven CO_2 reduction device. (b) Photovoltaic and electrocatalytic current density-voltage behaviors. (c) Selectivity toward CO, solar current density and solar-to-CO efficiency as a function of photoelectrolysis time. Reproduced with permission from Ref. [48]. Copyright 2017, Nature Publishing Group.

voltaics to construct a photovoltaic-based tandem electrocatalytic device for CO_2 reduction [47]. With IrO_2 as anode and oxidized Au as cathode, the device reached a solar-to-CO efficiency (SCOE) exceeding 6.5% with excellent stability over 18 h. However, hydrogen was still generated as a secondary product. To suppress the hydrogen evolution and overcome the limitation of noble metal catalyst, they chose earth–abundant catalyst (i.e., CuO nanowires with SnO_2 surface modification by atomic layer deposition) as both anode and cathode (Fig. 18a) [48]. The SnO_2 layer on surface could largely enhance the selectivity of CO production. Using a GaInP/GaInAs/Ge photovoltaic cell, the operating point of device well matched with the maximum power point of photovoltaic cell (Fig. 18b), ensuring the high energy utilization efficiency. As a result, a high SCOE of 13.4% with selectivity over 80% was achieved (Fig. 18c).

In addition, this concept was also applied to the combination of photoelectrodes. Most recently, Jing *et al.* [187] reported a PEC system for CO_2 reduction, which was composed of Nile red (NR_x) functionalized TiO_2 with Pd nanoparticles ($Pd/NR_x@TiO_2$) as photocathode and Co–Pi/W:$BiVO_4$ as photoanode. Their isotopic labelling experiments validated that CH_3OH was the main product and O_2 was simultaneously generated from water. Upon an external voltage of 0.6 V by a tandem Si-solar cell, the optimal system exhibited remarkable performance, yielding CH_3OH at a rate of 106 μmol L^{-1} h^{-1} cm^{-2} with a high apparent quantum efficiency (AQE) of up to 95%.

Wireless monolithic devices

The PEC setups for CO_2 reduction discussed in the preceding sections inevitably used a wire for the linkage between electrodes. Moreover, the electrodes generally are immersed in different electrolytes to optimize the reactions, which are separated by a proton exchange membrane to prevent the diffusion of products to opposite electrodes. In consideration of practical applications, the complex setups usually suffer from high cost and complicated operation. Enlightened by the leaf for photosynthesis, a wireless monolithic device has recently received appealing interest [188]. As shown in Fig. 19a, the semiconductor component for light harvesting is placed in the middle of device, and co-catalysts for reactions are anchored on two sides through conductive layers. This wireless device not only benefits from low cost and easy operation, but also can extend the application to complex environment such as sea water.

Another niche for this device is that the external electrical bias is no longer needed, avoiding the consumption

of electric energy. Since Nocera *et al.* introduced this concept into solar–driven water splitting to achieve an efficiency of 2.5% [189], the wireless device has also been exploited for CO_2 reduction by Arai and co-workers, as listed in Table 4. For instance, a Ru complex modified p-InP (InP/[RuCP]) was directly combined with a reduced $SrTiO_3$ (r-STO) to form a wireless system [132]. As depicted in Fig. 19b, profiting from the enlarged difference in the band-energy position between r-STO and InP, the electrons accumulated on the CB of InP and transferred to Ru complex, which performed the reduction of CO_2 to formate with a production amount of 0.94 μmol and SFE of 0.08% at no external electrical bias. Furthermore, they exploited an IrO_x/SiGe-jn/CC/p-RuCP wireless monolithic device for the reduction of CO_2 to formate [190]. The SFE was largely promoted up to 4.6% with 50.2 μmol of formate after irradiation of simulated solar light for 2 h.

Although the wireless monolithic devices have realized a photoelectrocatalytic process, it should be noted that the efficiency is lower than that by traditional wired setups, no matter for water splitting or CO_2 reduction [132,189]. A main reason is that the generated protons on photoanode must move around to photocathode on the back side (Fig. 19a). Compared with the wired setup, the relative long distance of ionic transport for the wireless device imposes tremendous ohmic losses [191]. Given this situation, further designs should be focused on the reduction of ionic transport distance, such as perforating semiconductors or constructing nanostructures. However, too short distance should also be avoided in order to successfully separate the products.

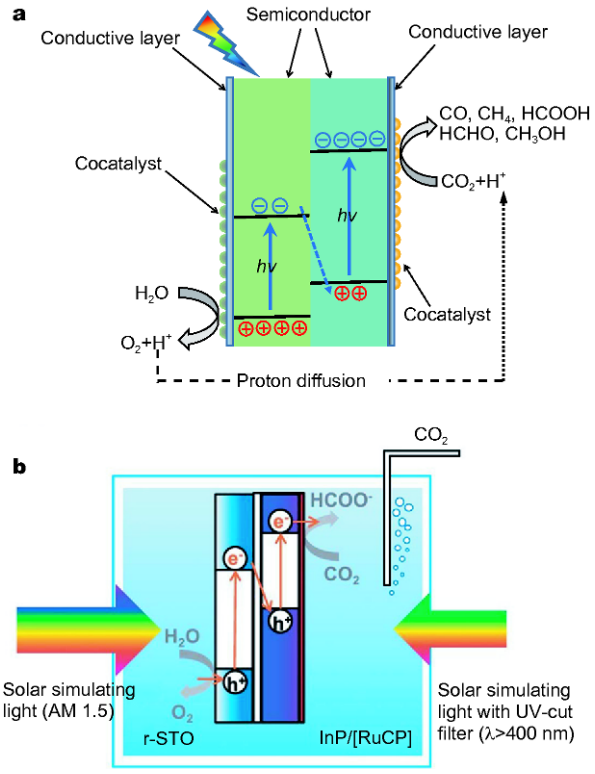

Figure 19 (a) Schematic representation for the electron and proton transport in wireless monolithic device for CO_2 reduction. (b) Schematic illustration for the r-STO/InP/[RuCP] wireless device for CO_2 reduction. Adapted with permission from Ref. [132]. Copyright 2013, the Royal Society of Chemistry.

SUMMARY AND PERSPECTIVES

The increasing energy crisis and global warming impel researchers to put emphasis on the unremitting exploitation of solar energy. Among diversiform applications, solar-driven CO_2 reduction shows several distinct advantages: 1) atmospheric CO_2 can be largely consumed to confront the unfavorable effect on global warming; 2) the reduction of CO_2 can generate various products, such as CO, HCOOH, CH_3OH and CH_4, which have widespread industry and energy applications; 3) solar energy can be stored in the chemical fuels with high-energy-density form. The photoelectrocatalysis, which integrates photocatalysis with electrocatalysis, can combine the merits of both approaches, endowing more remarkable performance. Recent several decades have witnessed the rapid developments of PEC CO_2 reduction, which have been systematically summarized and discussed in this review.

Considering that the photocathodes built by p-type semiconductors have been widely applied to CO_2 reduction, multifarious strategies are focused on constructing photocathodes, including improving light utilization efficiency and engineering high catalytic active sites. Thanks to the explosive development of solid-state physics and nanotechnology, a giant amount of strategies can be employed to revolutionize the photocathode toward high efficiency of light utilization, providing prerequisite to chemical reactions. The strategies of constructing 1D nanostructures, doping and forming heterojunctions are emphatically outlined in this review for modifying the band gap structure and altering the range of light absorption. These delicate designs for photocathodes at nanometer precision can intrinsically extend light absorption and facilitate charge separation and migration, which allows delivering sufficient energy and electrons for CO_2 activation and conversion. After ensuring the high efficiency of light utilization, anchoring co-catalysts with high catalytic activity of CO_2 reduction (e.g., metal

nanoparticles, homogeneous metal complexes, organic molecules such as protonated pyridine, conductive polymers and enzymatic biocatalysts) on photocathodes are underlined to confront the frustrating activity of semiconductor and the sluggish reactions. The anchored co-catalysts can lower the overpotential and reduce the energy barrier, facilitating CO_2 activation and conversion. Meanwhile, reduction pathways can also be specifically designated, providing an opportunity for tuning the selectivity of reactions.

In addition to modulating the photocathodes, researchers also put emphasis on another fascinating approach constructing novel setups for PEC CO_2 reduction for surmounting the intrinsic disadvantages of p-type semiconductors. The use of n-type semiconductor as photoanode can separate light-harvesting centers from catalytic sites, endowing the flexibility of optimizing their performance.

In the meantime, some novel setups infuse new blood for improving the efficiency of PEC CO_2 reduction. Combining photoanode with photocathode to construct a Z-scheme photocatalytic system cannot only expand the library of candidates to numerous semiconductors with narrow band gaps, but also supply a larger self-generated voltage to minimize the consumption of external electricity. It is worth mentioning that the dilemma between extending light absorption and matching redox potentials can be alleviated by another appealing device, which integrates a photovoltaic solar cell with the high effective electrocatalytic electrodes. In parallel, a wireless monolithic device has also specifically been developed to achieve low cost and easy operation.

In spite of the tremendous efforts and glorious achievements, the studies in this area are still in preliminary and many challenges are needed to confront. In fact, PEC CO_2 reduction suffers from a serious of scientific challenges, including high overpotential, low catalytic activity, poor product selectivity, and unsatisfactory catalyst stability. More importantly, the reaction mechanism is still ambiguous so that the systematic understanding should be urgently established to guide the subtle designs. As compared with the photocatalytic system with a suspension of photocatalyst particles in a solvent, the mass transfer in a PEC cell system is a key process as the reactions only proceed at the surface of photoelectrode, which largely limits the overall catalytic performance. In addition, the setups for PEC CO_2 reduction are much more complicated so as to suffer from higher operating costs, hindering the further practical application. Optimistically speaking, the remaining challenges provide us many opportunities for exploiting more efficient materials toward PEC CO_2 reduction. Herein, we highlight several aspects for PEC CO_2 reduction, which should be emphatically considered for further development in the future.

1) Improving the efficiency of CO_2 reduction. High efficiency of light utilization should be preferentially ensured to supply sufficient electrons for subsequent reactions, by extending light absorption as well as improving charge separation and migration. Borrowing from the glorious achievements in photocatalysis and photovoltaics, these matters can be well handled. The overpotential of reactions plays a crucial role in affecting the efficiency of CO_2 reduction. Constructing high active sites is an appealing strategy for lowering the overpotential, for which heterogeneous or homogeneous cocatalysts are commonly anchored on photoelectrodes. Given that diversiform co-catalysts have been subtly designed and exploited until now, a present challenge to overcome is how to modulate the integration of electrode with co-catalyst for efficient charge transfer and to avoid the deactivation for high stability.

In terms of heterogeneous cocatalysts, surface and interface engineering endows a promising approach to fabricate the catalytic system with high performance [111,192,193]. Generally speaking, surface engineering can alter the adsorption and desorption of substrate, intermediate and product molecules by tailoring the surface electronic state and configuration of catalytic sites, while the charge transfer and separation are largely influenced by interface engineering. To synergistically take advantage of surface and interface engineering, careful design must be implemented in the material synthesis. Several parameters such as facets, composition and defects can influence the behaviors at the surface and interface, which should be taken into consideration. For engineering homogeneous catalysts, one crucial factor is to furnish the strong connection without deactivating their catalytic activity [5]. Weak connection not only impedes the charge transfer, but also facilitates the shed of co-catalyst from electrode, quenching their activity. Notably atomically dispersed metal catalysts are highly recommended for the application in PEC CO_2 reduction owing to their superb catalytic activity. The strong anchoring of atomically dispersed metals to photoelectrodes is essentially required; otherwise, the aggregation of metal atoms will dramatically deactivate the activity.

2) Enhancing the selectivity of desirable products, especially for high-valuable products. The use of co-catalysts seems to be a competent approach to boost the

performance of CO_2 reduction. However, the competitive water reduction is more thermodynamically and kinetically favorable with the assistance of co-catalysts, largely impeding CO_2 reduction. It is almost impossible to completely eliminate the hydrogen evolution in the protonic electrolyte no matter for photocatalysis or electrocatalysis. An alternative way to avoid hydrogen evolution is to replace the protonic electrolyte with aprotic solvent such as CH_3CN and DMF; however, the product for CO_2 reduction is CO in this case, and hydrogenation reactions cannot occur owing to the absence of protons [27]. In fact, the hydrogen evolution is not good-for-nothing during CO_2 reduction process. If the product of CO_2 reduction is CO by excluding other components, a mixture gas of CO and H_2 will be obtained to form so-called syngas. The syngas is an industrial feedstock, as light olefins can be directly synthesized by the well-known Fischer-Tropsch synthesis using syngas as raw material. In view of this matter, a fascinating approach is to regulate the ratio of CO to H_2 in the products [194,195]. In comparison of eliminating the hydrogen evolution, this approach is well performed and endows more valuable products.

Among various products of CO_2 reduction, CO and HCOOH are much more favorable than the high-value products containing rich energy (e.g., CH_3OH, CH_4 and other light hydrocarbons) due to kinetic accessibility. Some robust catalysts for CO_2 reduction (e.g., homogeneous metal complexes) exhibit outstanding performance for CO evolution, but they are feeble for further reduction and hydrogenation. The exploitation of catalysts with high selectivity for the energy-rich chemicals is an urgent challenge. Here we name two candidates for this requirement which may boost the development in the future. One is Cu-based catalysts [114,121,122]. Many studies have revealed that Cu-based catalysts can yield deep-reduced products with high selectivity. Although the reaction pathways and intermediates are still controversial, the Cu-based catalysts hold the promise for future development. The other candidate is enzymatic biocatalysts [162,165]. The enzymatic biocatalysts typically show high selectivity for products without side reactions; however, high cost and poor stability hinder their further practical application, which should be emphatically considered. In addition to direct reduction, PEC CO_2 fixation in organic synthesis is also a promising approach to utilize solar energy and convert CO_2 to high-value chemicals [196].

3) Deeply and systematically understanding the sophisticated mechanisms of CO_2 reduction. Due to the complicated reaction pathways, the mechanism investigation of CO_2 reduction is still in preliminary. The insight of reaction pathways would greatly help the subtle design of catalysts. In a typical case, in terms of two-electron reduction products (i.e., CO and HCOOH), holding the $COOH^*$ intermediate and reducing the adsorption ability of CO on catalyst facilitate the evolution of CO, while the strong binding with $CO_2^{\bullet-}$ tends to enable a favorable HCOOH production [42].

Two key factors are emphasized for mechanism investigation: confirmation of catalytic sites and understanding of intermediates. Thanks to the recent explosive developments of advanced characterization techniques, the factors can be carefully investigated. For instance, X-ray absorption fine structure (XAFS) spectra can depict the geometries, electronic features, atomic distances and coordination environment at atomic precision [197,198], and aberration-corrected high-angle annular dark-field scanning transmission electron microscopy (HAADF-STEM) can distinctly photograph metal atoms [199], providing a powerful tool to dissect catalytic sites. Meanwhile, *in situ* characterization techniques (e.g., *in situ* Fourier transform infrared spectroscopy (FTIR) [200] and Raman spectroscopy [201]) can offer valuable information for the adsorbed carbon species and intermediates on the catalysts, which would guide us to depict the reaction pathways.

Overall, PEC CO_2 reduction offers a powerful tool to utilize the solar energy and to enable the conversion of CO_2 to fuels. To overcome the bottlenecks in this field, significant developments have been performed, including multifarious strategies and novel constructed setups. As a matter of fact, the exploitation of PEC CO_2 reduction is still in its early stage, and there is still a long way to its large-scale practical applications. We highlight the perspective that PEC CO_2 reduction will undergo the explosive developments to satisfy the human's demands for energy and environment.

Received 28 September 2017; accepted 26 October 2017; published online 31 January 2018

1 Schultz DM, Yoon TP. Solar synthesis: prospects in visible light photocatalysis. Science, 2014, 343: 1239176–1239176
2 Yoon TP, Ischay MA, Du J. Visible light photocatalysis as a greener approach to photochemical synthesis. Nat Chem, 2010, 2: 527–532
3 Brongersma ML, Halas NJ, Nordlander P. Plasmon-induced hot carrier science and technology. Nat Nanotechnol, 2015, 10: 25–34
4 Bai S, Jiang J, Zhang Q, *et al.* Steering charge kinetics in photocatalysis: intersection of materials syntheses, characterization techniques and theoretical simulations. Chem Soc Rev, 2015, 44:

2893–2939
5 Gao C, Wang J, Xu H, *et al.* Coordination chemistry in the design of heterogeneous photocatalysts. Chem Soc Rev, 2017, 46: 2799–2823
6 Kubacka A, Fernández–García M, Colón G. Advanced nanoarchitectures for solar photocatalytic applications. Chem Rev, 2012, 112: 1555–1614
7 Grätzel M. Photoelectrochemical cells. Nature, 2001, 414: 338–344
8 Walter MG, Warren EL, McKone JR, *et al.* Solar water splitting cells. Chem Rev, 2010, 110: 6446–6473
9 Kang D, Kim TW, Kubota SR, *et al.* Electrochemical synthesis of photoelectrodes and catalysts for use in solar water splitting. Chem Rev, 2015, 115: 12839–12887
10 Chen X, Shen S, Guo L, *et al.* Semiconductor-based photocatalytic hydrogen generation. Chem Rev, 2010, 110: 6503–6570
11 Ran J, Zhang J, Yu J, *et al.* Earth-abundant cocatalysts for semiconductor-based photocatalytic water splitting. Chem Soc Rev, 2014, 43: 7787–7812
12 Tachibana Y, Vayssieres L, Durrant JR. Artificial photosynthesis for solar water-splitting. Nat Photonics, 2012, 6: 511–518
13 White JL, Baruch MF, Pander III JE, *et al.* Light-driven heterogeneous reduction of carbon dioxide: photocatalysts and photoelectrodes. Chem Rev, 2015, 115: 12888–12935
14 Habisreutinger SN, Schmidt-Mende L, Stolarczyk JK. Photocatalytic reduction of CO_2 on TiO_2 and other semiconductors. Angew Chem Int Ed, 2013, 52: 7372–7408
15 Chang X, Wang T, Gong J. CO_2 photo-reduction: insights into CO_2 activation and reaction on surfaces of photocatalysts. Energy Environ Sci, 2016, 9: 2177–2196
16 Tu W, Zhou Y, Zou Z. Photocatalytic conversion of CO_2 into renewable hydrocarbon fuels: state-of-the-art accomplishment, challenges, and prospects. Adv Mater, 2014, 26: 4607–4626
17 Li X, Wen J, Low J, *et al.* Design and fabrication of semiconductor photocatalyst for photocatalytic reduction of CO_2 to solar fuel. Sci China Mater, 2014, 57: 70–100
18 Inoue T, Fujishima A, Konishi S, *et al.* Photoelectrocatalytic reduction of carbon dioxide in aqueous suspensions of semiconductor powders. Nature, 1979, 277: 637–638
19 Oh Y, Hu X. Organic molecules as mediators and catalysts for photocatalytic and electrocatalytic CO_2 reduction. Chem Soc Rev, 2013, 42: 2253–2261
20 Roger I, Shipman MA, Symes MD. Earth-abundant catalysts for electrochemical and photoelectrochemical water splitting. Nat Rev Chem, 2017, 1: 0003
21 Paracchino A, Laporte V, Sivula K, *et al.* Highly active oxide photocathode for photoelectrochemical water reduction. Nat Mater, 2011, 10: 456–461
22 Ji L, McDaniel M D, Wang S, *et al.* A silicon-based photocathode for water reduction with an epitaxial $SrTiO_3$ protection layer and a nanostructured catalyst. Nat Nanotechnol, 2014, 10: 84–90
23 Kim TW, Choi KS. Nanoporous $BiVO_4$ photoanodes with dual-layer oxygen evolution catalysts for solar water splitting. Science, 2014, 343: 990–994
24 Hu S, Shaner MR, Beardslee JA, *et al.* Amorphous TiO_2 coatings stabilize Si, GaAs, and GaP photoanodes for efficient water oxidation. Science, 2014, 344: 1005–1009
25 Hisatomi T, Kubota J, Domen K. Recent advances in semiconductors for photocatalytic and photoelectrochemical water splitting. Chem Soc Rev, 2014, 43: 7520–7535
26 Halmann M. Photoelectrochemical reduction of aqueous carbon dioxide on p–type gallium phosphide in liquid junction solar cells. Nature, 1978, 275: 115–116
27 Kumar B, Llorente M, Froehlich J, *et al.* Photochemical and Photoelectrochemical Reduction of CO_2. Annu Rev Phys Chem, 2012, 63: 541–569
28 Xie S, Zhang Q, Liu G, *et al.* Photocatalytic and photoelectrocatalytic reduction of CO_2 using heterogeneous catalysts with controlled nanostructures. Chem Commun, 2016, 52: 35–59
29 Choi SK, Kang U, Lee S, *et al.* Sn-coupled p-Si nanowire arrays for solar formate production from CO_2. Adv Energy Mater, 2014, 4: 1301614
30 LaTempa TJ, Rani S, Bao N, *et al.* Generation of fuel from CO_2 saturated liquids using a p-Si nanowire||n-TiO_2 nanotube array photoelectrochemical cell. Nanoscale, 2012, 4: 2245–2250
31 Chang X, Wang T, Zhang P, *et al.* Stable aqueous photoelectrochemical CO_2 reduction by a Cu_2O dark cathode with improved selectivity for carbonaceous products. Angew Chem Int Ed, 2016, 55: 8840–8845
32 Bachmeier A, Hall S, Ragsdale SW, *et al.* Selective visible-light-driven CO_2 Reduction on a p-type dye-sensitized NiO photocathode. J Am Chem Soc, 2014, 136: 13518–13521
33 Schreier M, Luo J, Gao P, *et al.* Covalent immobilization of a molecular catalyst on Cu_2O photocathodes for CO_2 reduction. J Am Chem Soc, 2016, 138: 1938–1946
34 Arai T, Tajima S, Sato S, *et al.* Selective CO_2 conversion to formate in water using a CZTS photocathode modified with a ruthenium complex polymer. Chem Commun, 2011, 47: 12664–12666
35 Yuan J, Hao C. Solar-driven photoelectrochemical reduction of carbon dioxide to methanol at $CuInS_2$ thin film photocathode. Sol Energy Mater Sol Cells, 2013, 108: 170–174
36 Jang YJ, Jang JW, Lee J, *et al.* Selective CO production by Au coupled ZnTe/ZnO in the photoelectrochemical CO_2 reduction system. Energy Environ Sci, 2015, 8: 3597–3604
37 Jang JW, Cho S, Magesh G, *et al.* Aqueous-solution route to zinc telluride films for application to CO_2 reduction. Angew Chem Int Ed, 2014, 53: 5852–5857
38 Zeng G, Qiu J, Li Z, *et al.* CO_2 reduction to methanol on TiO_2-passivated GaP photocatalysts. ACS Catal, 2014, 4: 3512–3516
39 Lessio M, Carter E A. What is the role of pyridinium in pyridine-catalyzed CO_2 reduction on p-GaP photocathodes? J Am Chem Soc, 2015, 137: 13248–13251
40 Kang U, Choi SK, Ham DJ, *et al.* Photosynthesis of formate from CO_2 and water at 1% energy efficiency *via* copper iron oxide catalysis. Energy Environ Sci, 2015, 8: 2638–2643
41 Sagara N, Kamimura S, Tsubota T, *et al.* Photoelectrochemical CO_2 reduction by a p-type boron-doped g-C_3N_4 electrode under visible light. Appl Catal B-Environ, 2016, 192: 193–198
42 Yang C, Yu X, Heißler S, *et al.* Surface faceting and reconstruction of ceria nanoparticles. Angew Chem Int Ed, 2017, 56: 375–379
43 Zhang Y, Luc W, Hutchings GS, *et al.* Photoelectrochemical carbon dioxide reduction using a nanoporous Ag cathode. ACS Appl Mater Interfaces, 2016, 8: 24652–24658
44 Magesh G, Kim ES, Kang HJ, *et al.* A versatile photoanode-driven photoelectrochemical system for conversion of CO_2 to fuels with high faradaic efficiencies at low bias potentials. J Mater Chem A, 2014, 2: 2044–2049
45 Sato S, Arai T, Morikawa T, *et al.* Selective CO_2 conversion to

formate conjugated with H_2O oxidation utilizing semiconductor/complex hybrid photocatalysts. J Am Chem Soc, 2011, 133: 15240–15243
46 Sahara G, Kumagai H, Maeda K, *et al.* Photoelectrochemical reduction of CO_2 coupled to water oxidation using a photocathode with a Ru(II)-Re(I) complex photocatalyst and a CoO_x/TaON photoanode. J Am Chem Soc, 2016, 138: 14152–14158
47 Schreier M, Curvat L, Giordano F, *et al.* Efficient photosynthesis of carbon monoxide from CO_2 using perovskite photovoltaics. Nat Commun, 2015, 6: 7326
48 Schreier M, Héroguel F, Steier L, *et al.* Solar conversion of CO_2 to CO using earth-abundant electrocatalysts prepared by atomic layer modification of CuO. Nat Energ, 2017, 2: 17087
49 Bolton J R. Solar Fuels. Science, 1978, 202: 705–711
50 Qiao J, Liu Y, Hong F, *et al.* A review of catalysts for the electroreduction of carbon dioxide to produce low-carbon fuels. Chem Soc Rev, 2014, 43: 631–675
51 Hong J, Zhang W, Ren J, *et al.* Photocatalytic reduction of CO_2: a brief review on product analysis and systematic methods. Anal Methods, 2013, 5: 1086
52 Surdhar PS, Mezyk SP, Armstrong DA. Reduction potential of the carboxyl radical anion in aqueous solutions. J Phys Chem, 1989, 93: 3360–3363
53 Huynh MHV, Meyer TJ. Proton-coupled electron transfer. Chem Rev, 2007, 107: 5004–5064
54 Costentin C, Robert M, Savéant JM. Catalysis of the electrochemical reduction of carbon dioxide. Chem Soc Rev, 2013, 42: 2423–2436
55 Ji Y, Luo Y. Theoretical study on the mechanism of photoreduction of CO_2 to CH_4 on the anatase TiO_2 (101) surface. ACS Catal, 2016, 6: 2018–2025
56 Neaţu Ş, Maciá–Agulló JA, Concepción P, *et al.* Gold-copper nanoalloys supported on TiO_2 as photocatalysts for CO_2 reduction by water. J Am Chem Soc, 2014, 136: 15969–15976
57 Kang Q, Wang T, Li P, *et al.* Photocatalytic reduction of carbon dioxide by hydrous hydrazine over Au-Cu alloy nanoparticles supported on $SrTiO_3$/TiO_2 coaxial nanotube arrays. Angew Chem Int Ed, 2015, 54: 841–845
58 Gao C, Meng Q, Zhao K, *et al.* Co_3O_4 hexagonal platelets with controllable facets enabling highly efficient visible-light photocatalytic reduction of CO_2. Adv Mater, 2016, 28: 6485–6490
59 Shown I, Hsu HC, Chang YC, *et al.* Highly efficient visible light photocatalytic reduction of CO_2 to hydrocarbon fuels by Cu-nanoparticle decorated graphene oxide. Nano Lett, 2014, 14: 6097–6103
60 Hori Y, Kikuchi K, Murata A, *et al.* Production of methane and ethylene in electrochemical reduction of carbon dioxide at copper electrode in aqueous hydrogencarbonate solution. Chem Lett, 1986, 15: 897–898
61 Cook RL. Photoelectrochemical carbon dioxide reduction to hydrocarbons at ambient temperature and pressure. J Electrochem Soc, 1988, 135: 3069–3070
62 Hirota K, Tryk DA, Yamamoto T, *et al.* Photoelectrochemical reduction of CO_2 in a high-pressure CO_2 + methanol medium at p-type semiconductor electrodes. J Phys Chem B, 1998, 102: 9834–9843
63 Hirota K. Photoelectrochemical reduction of CO_2 at high current densities at p-InP electrodes. J Electrochem Soc, 1998, 145: L82
64 Mikkelsen M, Jørgensen M, Krebs FC. The teraton challenge. A review of fixation and transformation of carbon dioxide. Energy Environ Sci, 2010, 3: 43–81
65 de Brito JF, Araujo AR, Rajeshwar K, *et al.* Photoelectrochemical reduction of CO_2 on Cu/Cu_2O films: product distribution and pH effects. Chem Eng J, 2015, 264: 302–309
66 Zou X, Zhang Y. Noble metal-free hydrogen evolution catalysts for water splitting. Chem Soc Rev, 2015, 44: 5148–5180
67 Hara K. High efficiency electrochemical reduction of carbon dioxide under high pressure on a gas diffusion electrode containing Pt catalysts. J Electrochem Soc, 1995, 142: L57
68 Miller MB, Chen DL, Luebke DR, *et al.* Critical assessment of CO_2 solubility in volatile solvents at 298.15 K. J Chem Eng Data, 2011, 56: 1565–1572
69 Kaneco S, Katsumata H, Suzuki T, *et al.* Photoelectrocatalytic reduction of CO_2 in LiOH/methanol at metal-modified p-InP electrodes. Appl Catal B-Environ, 2006, 64: 139–145
70 Kou Y, Nakatani S, Sunagawa G, *et al.* Visible light-induced reduction of carbon dioxide sensitized by a porphyrin-rhenium dyad metal complex on p-type semiconducting NiO as the reduction terminal end of an artificial photosynthetic system. J Catal, 2014, 310: 57–66
71 Medina–Ramos J, Pupillo RC, Keane TP, *et al.* Efficient conversion of CO_2 to CO using tin and other inexpensive and easily prepared post-transition metal catalysts. J Am Chem Soc, 2015, 137: 5021–5027
72 Lin J, Ding Z, Hou Y, *et al.* Ionic liquid co-catalyzed artificial photosynthesis of CO. Sci Rep, 2013, 3: 1056
73 Rosen BA, Salehi–Khojin A, Thorson MR, *et al.* Ionic liquid-mediated selective conversion of CO_2 to CO at low overpotentials. Science, 2011, 334: 643–644
74 Lu W, Jia B, Cui B, et al. Efficient photoelectrochemical reduction of CO_2 to formic acid with functionalized ionic liquid as absorbent and electrolyte. Angew Chem Int Ed, 2017, 56: 11851–11854
75 Choi CH, Chung J, Woo SI. Photoelectrochemical production of formic acid and methanol from carbon dioxide on metal-decorated CuO/Cu_2O-layered thin films under visible light irradiation. Appl Catal B, 2014, 158-159: 217–223
76 Shen Q, Chen Z, Huang X, *et al.* High-yield and selective photoelectrocatalytic reduction of CO_2 to formate by metallic copper decorated Co_3O_4 nanotube arrays. Environ Sci Technol, 2015, 49: 5828–5835
77 Tong H, Ouyang S, Bi Y, *et al.* Nano-photocatalytic materials: possibilities and challenges. Adv Mater, 2012, 24: 229–251
78 Liu S, Tang ZR, Sun Y, *et al.* One-dimension-based spatially ordered architectures for solar energy conversion. Chem Soc Rev, 2015, 44: 5053–5075
79 Dasgupta NP, Sun J, Liu C, *et al.* 25th anniversary article: semiconductor nanowires-synthesis, characterization, and applications. Adv Mater, 2014, 26: 2137–2184
80 Xie JL, Guo CX, Li CM. Construction of one-dimensional nanostructures on graphene for efficient energy conversion and storage. Energy Environ Sci, 2014, 7: 2559–2579
81 Hochbaum A I, Yang P. Semiconductor nanowires for energy conversion. Chem Rev, 2010, 110: 527–546
82 Ghadimkhani G, de Tacconi NR, Chanmanee W, *et al.* Efficient solar photoelectrosynthesis of methanol from carbon dioxide using hybrid CuO-Cu_2O semiconductor nanorod arrays. Chem Commun, 2013, 49: 1297–1299
83 Rajeshwar K, de Tacconi NR, Ghadimkhani G, *et al.* Tailoring copper oxide semiconductor nanorod arrays for photoelectrochemical reduction of carbon dioxide to methanol. Chem-

PhysChem, 2013, 14: 2251–2259
84 Sun K, Shen S, Liang Y, *et al.* Enabling silicon for solar-fuel production. Chem Rev, 2014, 114: 8662–8719
85 Asahi R, Morikawa T, Ohwaki T, *et al.* Visible-light photocatalysis in nitrogen-doped titanium oxides. Science, 2001, 293: 269–271
86 Shen S, Zhao L, Zhou Z, *et al.* Enhanced photocatalytic hydrogen evolution over Cu-doped $ZnIn_2S_4$ under visible light irradiation. J Phys Chem C, 2008, 112: 16148–16155
87 Liu B, Chen HM, Liu C, *et al.* Large-scale synthesis of transition-metal-doped TiO_2 nanowires with controllable overpotential. J Am Chem Soc, 2013, 135: 9995–9998
88 Nasution H, Purnama E, Kosela S, *et al.* Photocatalytic reduction of CO on copper-doped titania catalysts prepared by improved-impregnation method. Catal Commun, 2005, 6: 313–319
89 Wang G, Yang Y, Han D, *et al.* Oxygen defective metal oxides for energy conversion and storage. Nano Today, 2017, 13: 23–39
90 Chen X, Liu L, Huang F. Black titanium dioxide (TiO_2) nanomaterials. Chem Soc Rev, 2015, 44: 1861–1885
91 Han T, Chen Y, Tian G, *et al.* Hydrogenated TiO_2/$SrTiO_3$ porous microspheres with tunable band structure for solar-light photocatalytic H_2 and O_2 evolution. Sci China Mater, 2016, 59: 1003–1016
92 Zuo F, Bozhilov K, Dillon RJ, *et al.* Active facets on titanium(III)-doped TiO_2: an effective strategy to improve the visible-light photocatalytic activity. Angew Chem Int Ed, 2012, 51: 6223–6226
93 Lee J, Sorescu DC, Deng X. Electron-induced dissociation of CO_2 on TiO_2 (110). J Am Chem Soc, 2011, 133: 10066–10069
94 Zhang N, Li X, Ye H, *et al.* Oxide defect engineering enables to couple solar energy into oxygen activation. J Am Chem Soc, 2016, 138: 8928–8935
95 Gu J, Wuttig A, Krizan JW, *et al.* Mg-doped $CuFeO_2$ photocathodes for photoelectrochemical reduction of carbon dioxide. J Phys Chem C, 2013, 117: 12415–12422
96 Peng H, Lu J, Wu C, *et al.* Co-doped MoS_2 NPs with matched energy band and low overpotential high efficiently convert CO_2 to methanol. Appl Surf Sci, 2015, 353: 1003–1012
97 Xi G, Ouyang S, Li P, *et al.* Ultrathin $W_{18}O_{49}$ nanowires with diameters below 1 nm: synthesis, near-infrared absorption, photoluminescence, and photochemical reduction of carbon dioxide. Angew Chem Int Ed, 2012, 51: 2395–2399
98 Liu L, Jiang Y, Zhao H, *et al.* Engineering coexposed {001} and {101} facets in oxygen-deficient TiO_2 nanocrystals for enhanced CO_2 photoreduction under visible light. ACS Catal, 2016, 6: 1097–1108
99 Ma M, Zhang K, Li P, *et al.* Dual oxygen and tungsten vacancies on a WO_3 photoanode for enhanced water oxidation. Angew Chem Int Ed, 2016, 55: 11819–11823
100 Gao S, Sun Y, Lei F, *et al.* Freestanding atomically-thin cuprous oxide sheets for improved visible-light photoelectrochemical water splitting. Nano Energy, 2014, 8: 205–213
101 Li H, Shang J, Ai Z, *et al.* Efficient visible light nitrogen fixation with biobr nanosheets of oxygen vacancies on the exposed {001} facets. J Am Chem Soc, 2015, 137: 6393–6399
102 Qu Y, Duan X. Progress, challenge and perspective of heterogeneous photocatalysts. Chem Soc Rev, 2013, 42: 2568–2580
103 Wu F, Cao F, Liu Q, *et al.* Enhancing photoelectrochemical activity with three-dimensional p-CuO/n-ZnO junction photocathodes. Sci China Mater, 2016, 59: 825–832
104 Janáky C, Hursán D, Endrődi B, *et al.* Electro- and photoreduction of carbon dioxide: the twain shall meet at copper oxide/copper interfaces. ACS Energy Lett, 2016, 1: 332–338
105 Garcia-Esparza AT, Limkrailassiri K, Leroy F, *et al.* Photoelectrochemical and electrocatalytic properties of thermally oxidized copper oxide for efficient solar fuel production. J Mater Chem A, 2014, 2: 7389–7401
106 Mahalingam T, John VS, Rajendran S, *et al.* Electrochemical deposition of ZnTe thin films. Semicond Sci Technol, 2002, 17: 465–470
107 Chen YW, Prange JD, Dühnen S, *et al.* Atomic layer-deposited tunnel oxide stabilizes silicon photoanodes for water oxidation. Nat Mater, 2011, 10: 539–544
108 Esposito DV, Levin I, Moffat TP, *et al.* H_2 evolution at Si-based metal-insulator-semiconductor photoelectrodes enhanced by inversion channel charge collection and H spillover. Nat Mater, 2013, 12: 562–568
109 Seger B, Pedersen T, Laursen AB, *et al.* Using TiO_2 as a conductive protective layer for photocathodic H_2 evolution. J Am Chem Soc, 2013, 135: 1057–1064
110 Schreier M, Gao P, Mayer MT, *et al.* Efficient and selective carbon dioxide reduction on low cost protected Cu_2O photocathodes using a molecular catalyst. Energ Environ Sci, 2015, 8: 855–861
111 Bai S, Yin W, Wang L, *et al.* Surface and interface design in cocatalysts for photocatalytic water splitting and CO_2 reduction. RSC Adv, 2016, 6: 57446–57463
112 Zhao J, Wang X, Xu Z, *et al.* Hybrid catalysts for photoelectrochemical reduction of carbon dioxide: a prospective review on semiconductor/metal complex co-catalyst systems. J Mater Chem A, 2014, 2: 15228–15233
113 Yang J, Wang D, Han H, *et al.* Roles of cocatalysts in photocatalysis and photoelectrocatalysis. Acc Chem Res, 2013, 46: 1900–1909
114 Kuhl KP, Hatsukade T, Cave ER, *et al.* Electrocatalytic conversion of carbon dioxide to methane and methanol on transition metal surfaces. J Am Chem Soc, 2014, 136: 14107–14113
115 Zhu W, Michalsky R, Metin Ö, *et al.* Monodisperse Au nanoparticles for selective electrocatalytic reduction of CO_2 to CO. J Am Chem Soc, 2013, 135: 16833–16836
116 Lu Q, Rosen J, Zhou Y, *et al.* A selective and efficient electrocatalyst for carbon dioxide reduction. Nat Commun, 2014, 5: 3242
117 Gao D, Zhou H, Wang J, *et al.* Size-dependent electrocatalytic reduction of CO_2 over Pd nanoparticles. J Am Chem Soc, 2015, 137: 4288–4291
118 Lei F, Liu W, Sun Y, *et al.* Metallic tin quantum sheets confined in graphene toward high-efficiency carbon dioxide electroreduction. Nat Commun, 2016, 7: 12697
119 Alvarez Guerra M, Quintanilla S, Irabien A. Conversion of carbon dioxide into formate using a continuous electrochemical reduction process in a lead cathode. Chem Eng J, 2012, 207-208: 278–284
120 Hou J, Cheng H, Takeda O, *et al.* Three-dimensional bimetal-graphene-semiconductor coaxial nanowire arrays to harness charge flow for the photochemical reduction of carbon dioxide. Angew Chem Int Ed, 2015, 54: 8480–8484
121 Long R, Li Y, Liu Y, *et al.* Isolation of Cu atoms in Pd lattice: forming highly selective sites for photocatalytic conversion of CO_2 to CH_4. J Am Chem Soc, 2017, 139: 4486–4492
122 Kuhl KP, Cave ER, Abram DN, *et al.* New insights into the electrochemical reduction of carbon dioxide on metallic copper

surfaces. Energy Environ Sci, 2012, 5: 7050–7059
123 Hinogami R, Nakamura Y, Yae S, *et al.* An approach to ideal semiconductor electrodes for efficient photoelectrochemical reduction of carbon dioxide by modification with small metal particles. J Phys Chem B, 1998, 102: 974–980
124 Ikeda S, Saito Y, Yoshida M, *et al.* Photoelectrochemical reduction products of carbon dioxide at metal coated p-GaP photocathodes in non-aqueous electrolytes. J Electroanal Chem Interfacial Electrochem, 1989, 260: 335–345
125 Kaneco S, Ueno Y, Katsumata H, *et al.* Photoelectrochemical reduction of CO_2 at p-InP electrode in copper particle-suspended methanol. Chem Eng J, 2009, 148: 57–62
126 Morris AJ, Meyer GJ, Fujita E. Molecular approaches to the photocatalytic reduction of carbon dioxide for solar fuels. Acc Chem Res, 2009, 42: 1983–1994
127 Liu X, Inagaki S, Gong J. Heterogeneous molecular systems for photocatalytic CO_2 reduction with water oxidation. Angew Chem Int Ed, 2016, 55: 14924–14950
128 Kou Y, Nabetani Y, Masui D, *et al.* direct detection of key reaction intermediates in photochemical CO_2 reduction sensitized by a rhenium bipyridine complex. J Am Chem Soc, 2014, 136: 6021–6030
129 Kumar B, Smieja JM, Kubiak CP. Photoreduction of CO_2 on p-type silicon using Re(bipy-Bu^t)$(CO)_3$ Cl: photovoltages exceeding 600 mV for the selective reduction of CO_2 to CO. J Phys Chem C, 2010, 114: 14220–14223
130 Kumar B, Smieja JM, Sasayama AF, *et al.* Tunable, light-assisted co-generation of CO and H_2 from CO_2 and H_2O by Re(bipy-*t*bu)$(CO)_3$Cl and p-Si in non-aqueous medium. Chem Commun, 2012, 48: 272–274
131 Arai T, Sato S, Uemura K, *et al.* Photoelectrochemical reduction of CO_2 in water under visible-light irradiation by a p-type InP photocathode modified with an electropolymerized ruthenium complex. Chem Commun, 2010, 46: 6944–6946
132 Arai T, Sato S, Kajino T, *et al.* Solar CO_2 reduction using H_2O by a semiconductor/metal-complex hybrid photocatalyst: enhanced efficiency and demonstration of a wireless system using $SrTiO_3$ photoanodes. Energy Environ Sci, 2013, 6: 1274–1282
133 Ueda Y, Takeda H, Yui T, *et al.* A visible-light harvesting system for CO_2 reduction using a Ru^{II}-Re^{I} photocatalyst adsorbed in mesoporous organosilica. ChemSusChem, 2015, 8: 439–442
134 Sahara G, Abe R, Higashi M, *et al.* Photoelectrochemical CO_2 reduction using a Ru(ii)-Re(i) multinuclear metal complex on a p-type semiconducting NiO electrode. Chem Commun, 2015, 51: 10722–10725
135 Chen L, Guo Z, Wei X G, *et al.* Molecular catalysis of the electrochemical and photochemical reduction of CO_2 with earth-abundant metal complexes. Selective production of CO *vs* HCOOH by switching of the metal center. J Am Chem Soc, 2015, 137: 10918–10921
136 Thoi VS, Kornienko N, Margarit CG, *et al.* Visible-light photoredox catalysis: selective reduction of carbon dioxide to carbon monoxide by a nickel *N*-heterocyclic carbene-isoquinoline complex. J Am Chem Soc, 2013, 135: 14413–14424
137 Takeda H, Koizumi H, Okamoto K, *et al.* Photocatalytic CO_2 reduction using a Mn complex as a catalyst. Chem Commun, 2014, 50: 1491–1493
138 Bonin J, Robert M, Routier M. Selective and efficient photocatalytic CO_2 reduction to CO using visible light and an iron-based homogeneous catalyst. J Am Chem Soc, 2014, 136: 16768–16771
139 Alenezi K, Ibrahim SK, Li P, *et al.* Solar fuels: photoelectrosynthesis of CO from CO_2 at p-Type Si using Fe porphyrin electrocatalysts. Chem Eur J, 2013, 19: 13522–13527
140 Rosser TE, Windle CD, Reisner E. Electrocatalytic and solar-driven CO_2 reduction to CO with a molecular manganese catalyst immobilized on mesoporous TiO_2. Angew Chem Int Ed, 2016, 55: 7388–7392
141 Rao H, Schmidt LC, Bonin J, *et al.* Visible-light-driven methane formation from CO_2 with a molecular iron catalyst. Nature, 2017, 548: 74–77
142 Taniguchi I, Aurian-Blajeni B, Bockris J O M. Photo-aided reduction of carbon dioxide to carbon monoxide. J Electroanal Chem Interfacial Electrochem, 1983, 157: 179–182
143 Taniguchi I, Aurian–Blajeni B, Bockris JOM. The mediation of the photoelectrochemical reduction of carbon dioxide by ammonium ions. J Electroanal Chem Interfacial Electrochem, 1984, 161: 385–388
144 Bockris JOM. The photoelectrocatalytic reduction of carbon dioxide. J Electrochem Soc, 1989, 136: 2521–2528
145 Barton EE, Rampulla DM, Bocarsly AB. Selective solar-driven reduction of CO_2 to methanol using a catalyzed p-GaP based photoelectrochemical cell. J Am Chem Soc, 2008, 130: 6342–6344
146 Jeon JH, Mareeswaran PM, Choi CH, *et al.* Synergism between CdTe semiconductor and pyridine-photoenhanced electrocatalysis for CO_2 reduction to formic acid. RSC Adv, 2014, 4: 3016–3019
147 Keith JA, Carter EA. Electrochemical reactivities of pyridinium in solution: consequences for CO_2 reduction mechanisms. Chem Sci, 2013, 4: 1490–1496
148 Barton Cole E, Lakkaraju PS, Rampulla DM, *et al.* Using a one-electron shuttle for the multielectron reduction of CO_2 to methanol: kinetic, mechanistic, and structural insights. J Am Chem Soc, 2010, 132: 11539–11551
149 Keith JA, Carter EA. Theoretical insights into pyridinium-based photoelectrocatalytic reduction of CO_2. J Am Chem Soc, 2012, 134: 7580–7583
150 Keith J A, Carter E A. Theoretical insights into electrochemical CO_2 reduction mechanisms catalyzed by surface-bound nitrogen heterocycles. J Phys Chem Lett, 2013, 4: 4058–4063
151 Yan Y, Zeitler EL, Gu J, *et al.* Electrochemistry of aqueous pyridinium: exploration of a key aspect of electrocatalytic reduction of CO_2 to methanol. J Am Chem Soc, 2013, 135: 14020–14023
152 Lim CH, Holder AM, Musgrave CB. Mechanism of homogeneous reduction of CO_2 by pyridine: proton relay in aqueous solvent and aromatic stabilization. J Am Chem Soc, 2013, 135: 142–154
153 Lim CH, Holder AM, Hynes JT, *et al.* Reduction of CO_2 to methanol catalyzed by a biomimetic organo-hydride produced from pyridine. J Am Chem Soc, 2014, 136: 16081–16095
154 Dridi H, Comminges C, Morais C, *et al.* Catalysis and inhibition in the electrochemical reduction of CO_2 on platinum in the presence of protonated pyridine. New insights into mechanisms and products. J Am Chem Soc, 2017, 139: 13922–13928
155 Grace AN, Choi SY, Vinoba M, *et al.* Electrochemical reduction of carbon dioxide at low overpotential on a polyaniline/Cu_2O nanocomposite based electrode. Appl Energy, 2014, 120: 85–94
156 Aydin R, Dogan HO, Koleli F. Electrochemical reduction of carbondioxide on polypyrrole coated copper electro-catalyst under ambient and high pressure in methanol. Appl Catal B, 2013, 140-141: 478–482

157 Coskun H, Aljabour A, De Luna P, *et al.* Biofunctionalized conductive polymers enable efficient CO_2 electroreduction. Sci Adv, 2017, 3: e1700686
158 Won DH, Chung J, Park SH, *et al.* Photoelectrochemical production of useful fuels from carbon dioxide on a polypyrrole-coated p-ZnTe photocathode under visible light irradiation. J Mater Chem A, 2015, 3: 1089–1095
159 Guzmán D, Isaacs M, Osorio–Román I, *et al.* Photoelectrochemical reduction of carbon dioxide on quantum-dot-modified electrodes by electric field directed layer-by-layer assembly methodology. ACS Appl Mater Interfaces, 2015, 7: 19865–19869
160 Woolerton TW, Sheard S, Reisner E, *et al.* Efficient and clean photoreduction of CO_2 to CO by enzyme-modified TiO_2 nanoparticles using visible light. J Am Chem Soc, 2010, 132: 2132–2133
161 Reda T, Plugge CM, Abram NJ, *et al.* Reversible interconversion of carbon dioxide and formate by an electroactive enzyme. Proc Natl Acad Sci USA, 2008, 105: 10654–10658
162 Shi J, Jiang Y, Jiang Z, *et al.* Enzymatic conversion of carbon dioxide. Chem Soc Rev, 2015, 44: 5981–6000
163 Parkinson BA, Weaver PF. Photoelectrochemical pumping of enzymatic CO_2 reduction. Nature, 1984, 309: 148–149
164 Bachmeier A, Wang VCC, Woolerton TW, *et al.* How light-harvesting semiconductors can alter the bias of reversible electrocatalysts in favor of H_2 production and CO_2 reduction. J Am Chem Soc, 2013, 135: 15026–15032
165 Kuk SK, Singh RK, Nam DH, *et al.* Photoelectrochemical reduction of carbon dioxide to methanol through a highly efficient enzyme cascade. Angew Chem Int Ed, 2017, 56: 3827–3832
166 Jing L, Zhou W, Tian G, *et al.* Surface tuning for oxide-based nanomaterials as efficient photocatalysts. Chem Soc Rev, 2013, 42: 9509–9549
167 Huang Y, Yu Y, Xin Y, *et al.* Promoting charge carrier utilization by integrating layered double hydroxide nanosheet arrays with porous $BiVO_4$ photoanode for efficient photoelectrochemical water splitting. Sci China Mater, 2017, 60: 193–207
168 Bai Y, Mora–Seró I, De Angelis F, *et al.* Titanium dioxide nanomaterials for photovoltaic applications. Chem Rev, 2014, 114: 10095–10130
169 Cheng J, Zhang M, Wu G, *et al.* Photoelectrocatalytic reduction of CO_2 into chemicals using Pt-modified reduced graphene oxide combined with Pt-modified TiO_2 nanotubes. Environ Sci Technol, 2014, 48: 7076–7084
170 Cheng J, Zhang M, Wu G, *et al.* Optimizing CO_2 reduction conditions to increase carbon atom conversion using a Pt-RGO|| Pt-TNT photoelectrochemical cell. Sol Energ Mater Sol Cells, 2015, 132: 606–614
171 Cheng J, Zhang M, Liu J, *et al.* A Cu foam cathode used as a Pt-RGO catalyst matrix to improve CO_2 reduction in a photoelectrocatalytic cell with a TiO_2 photoanode. J Mater Chem A, 2015, 3: 12947–12957
172 Huang H, Jia H, Liu Z, *et al.* Understanding of strain effects in the electrochemical reduction of CO_2: using Pd nanostructures as an ideal platform. Angew Chem Int Ed, 2017, 56: 3594–3598
173 Zhao C, Dai X, Yao T, *et al.* Ionic exchange of metal-organic frameworks to access single nickel sites for efficient electroreduction of CO_2. J Am Chem Soc, 2017, 139: 8078–8081
174 Kim D, Xie C, Becknell N, *et al.* Electrochemical activation of CO_2 through atomic ordering transformations of AuCu nanoparticles. J Am Chem Soc, 2017, 139: 8329–8336
175 Gao D, Zhang Y, Zhou Z, *et al.* Enhancing CO_2 electroreduction with the metal-oxide interface. J Am Chem Soc, 2017, 139: 5652–5655
176 Zhu DD, Liu JL, Qiao SZ. Recent advances in inorganic heterogeneous electrocatalysts for reduction of carbon dioxide. Adv Mater, 2016, 28: 3423–3452
177 Gao S, Lin Y, Jiao X, *et al.* Partially oxidized atomic cobalt layers for carbon dioxide electroreduction to liquid fuel. Nature, 2016, 529: 68–71
178 Kumar B, Atla V, Brian JP, *et al.* Reduced SnO_2 porous nanowires with a high density of grain boundaries as catalysts for efficient electrochemical CO_2-into-HCOOH conversion. Angew Chem Int Ed, 2017, 56: 3645–3649
179 Asadi M, Kumar B, Behranginia A, *et al.* Robust carbon dioxide reduction on molybdenum disulphide edges. Nat Commun, 2014, 5: 4470
180 Chan K, Tsai C, Hansen HA, *et al.* Molybdenum sulfides and selenides as possible electrocatalysts for CO_2 reduction. ChemCatChem, 2014, 6: 1899–1905
181 Kumar B, Asadi M, Pisasale D, *et al.* Renewable and metal-free carbon nanofibre catalysts for carbon dioxide reduction. Nat Commun, 2013, 4: 2819
182 Wang H, Jia J, Song P, *et al.* Efficient electrocatalytic reduction of CO_2 by nitrogen-doped nanoporous carbon/carbon nanotube membranes: a step towards the electrochemical CO_2 refinery. Angew Chem Int Ed, 2017, 56: 7847–7852
183 Maeda K. Z-scheme water splitting using two different semiconductor photocatalysts. ACS Catal, 2013, 3: 1486–1503
184 Zhou P, Yu J, Jaroniec M. All-solid-state Z-scheme photocatalytic systems. Adv Mater, 2014, 26: 4920–4935
185 Winkler MT, Cox CR, Nocera DG, *et al.* Modeling integrated photovoltaic-electrochemical devices using steady-state equivalent circuits. Proc Natl Acad Sci USA, 2013, 110: E1076–E1082
186 Luo J, Im JH, Mayer MT, *et al.* Water photolysis at 12.3% efficiency *via* perovskite photovoltaics and earth-abundant catalysts. Science, 2014, 345: 1593–1596
187 Jia Y, Xu Y, Nie R, *et al.* Artificial photosynthesis of methanol from carbon dioxide and water *via* a Nile red-embedded TiO_2 photocathode. J Mater Chem A, 2017, 5: 5495–5501
188 Rongé J, Bosserez T, Martel D, *et al.* Monolithic cells for solar fuels. Chem Soc Rev, 2014, 43: 7963–7981
189 Reece SY, Hamel JA, Sung K, *et al.* Wireless solar water splitting using silicon-based semiconductors and earth-abundant catalysts. Science, 2011, 334: 645–648
190 Arai T, Sato S, Morikawa T. A monolithic device for CO_2 photoreduction to generate liquid organic substances in a single-compartment reactor. Energy Environ Sci, 2015, 8: 1998–2002
191 Haussener S, Xiang C, Spurgeon JM, *et al.* Modeling, simulation, and design criteria for photoelectrochemical water-splitting systems. Energy Environ Sci, 2012, 5: 9922–9935
192 Bai S, Wang L, Li Z, *et al.* Facet-engineered surface and interface design of photocatalytic materials. Adv Sci, 2017, 4: 1600216
193 Bai S, Xiong Y. Some recent developments in surface and interface design for photocatalytic and electrocatalytic hybrid structures. Chem Commun, 2015, 51: 10261–10271
194 Kang P, Chen Z, Nayak A, *et al.* Single catalyst electrocatalytic reduction of CO_2 in water to H_2+CO syngas mixtures with water oxidation to O_2. Energy Environ Sci, 2014, 7: 4007–4012
195 Ross MB, Dinh CT, Li Y, *et al.* Tunable Cu enrichment enables designer syngas electrosynthesis from CO_2. J Am Chem Soc, 2017,

139: 9359–9363
196 Liu R, Yuan G, Joe CL, *et al.* Silicon nanowires as photoelectrodes for carbon dioxide fixation. Angew Chem Int Ed, 2012, 51: 6709–6712
197 Sun Y, Gao S, Lei F, *et al.* Atomically-thin two-dimensional sheets for understanding active sites in catalysis. Chem Soc Rev, 2015, 44: 623–636
198 Frenkel AI. Applications of extended X-ray absorption fine-structure spectroscopy to studies of bimetallic nanoparticle catalysts. Chem Soc Rev, 2012, 41: 8163–8178
199 Akita T, Kohyama M, Haruta M. Electron microscopy study of gold nanoparticles deposited on transition metal oxides. Acc Chem Res, 2013, 46: 1773–1782
200 Wang Y, Wöll C. IR spectroscopic investigations of chemical and photochemical reactions on metal oxides: bridging the materials gap. Chem Soc Rev, 2017, 46: 1875–1932
201 Kim H, Kosuda KM, Van Duyne RP, *et al.* Resonance Raman and surface- and tip-enhanced Raman spectroscopy methods to study solid catalysts and heterogeneous catalytic reactions. Chem Soc Rev, 2010, 39: 4820–4844

Acknowledgements This work was financially supported in part by the National Key R&D Program of China (2017YFA0207301), the National Basic Research Program of China (973 Program, 2014CB848900), the National Natural Science Foundation of China (21471141 and U1532135), the CAS Key Research Program of Frontier Sciences (QYZDB-SSW-SLH018), the CAS Interdisciplinary Innovation Team, the Innovative Program of Development Foundation of Hefei Center for Physical Science and Technology (2016FXCX003), the Recruitment Program of Global Experts, the CAS Hundred Talent Program, Anhui Provincial Natural Science Foundation (1708085QB26), China Postdoctoral Science Foundation (BH2060000034), and the Fundamental Research Funds for the Central Universities (WK2060190064).

Author contributions Zhang N prepared the figures and wrote the paper. Xiong Y proposed and guided the project. Gao C, Long R, and Xiong Y revised the manuscript. All authors joined the discussion and gave useful suggestions.

Conflict of interest The authors declare that they have no conflict of interest.

Ning Zhang received his BSc in chemistry in 2013 from the University of Science and Technology of China (USTC). Since then he has been studying as a PhD candidate under the tutelage of Professor Yujie Xiong at USTC. His research interests focus on the controlled synthesis of semiconductors and their applications of photocatalysis and photoelectrocatalysis.

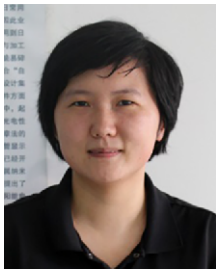

Ran Long received her BSc in chemistry in 2009 and PhD in inorganic chemistry under the tutelage of Professor Yujie Xiong in 2014, both from USTC. She is currently a research associate professor at USTC. Her research interests focus on the controlled synthesis and catalytic applications of metal nanocrystals.

Chao Gao received his BSc in chemistry in 2010 from Anhui Normal University, and PhD in inorganic chemistry in 2015 (with Professors Xingjiu Huang and Zhiyong Tang) from USTC. During his PhD research, he had two-year training (2013–2015) with Professor Zhiyong Tang at the National Center for Nanoscience and Technology (NCNST). He is now working as a postdoctoral research fellow with Professor Yujie Xiong at USTC. His current research interests are focused on the design and synthesis of photocatalysts and photoelectrodes for CO_2 reduction.

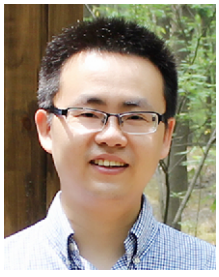

Yujie Xiong received his BSc in chemical physics in 2000 and PhD in inorganic chemistry under the tutelage of Professor Yi Xie in 2004, both from USTC. After four-year training with Professors Younan Xia and John A. Rogers, he joined the National Nanotechnology Infrastructure Network (NSF-NNIN), and served as the Principal Scientist and Lab Manager at Washington University in St. Louis. In 2011, he moved to USTC to take the position of professor of chemistry. His research interests include the synthesis, fabrication and assembly of inorganic materials for energy and environmental applications.

用于光电催化还原CO_2为燃料的设计进展

张宁, 龙冉, 高超*, 熊宇杰*

摘要 当今能源危机以及全球温室效应日益严重. 以太阳能驱动的CO_2还原为解决这些问题提供了一个全新的绿色途径, 并受到研究者的广泛关注. 光电催化过程能够整合光催化和电催化两者的优势, 从而实现对CO_2还原更高的效率和更理想的选择性. 近几十年来, 光电催化CO_2还原蓬勃发展, 已经取得了一些令人瞩目的成果. 本文总结了近年来基于光电催化CO_2还原的设计工作. 在讨论CO_2还原的基本理论和评价体系的基础上, 我们首先介绍了光阴极的调控手段, 包括提高光利用效率、开拓催化活性位点、调控反应过程等等. 此外, 我们还讨论了最近发展的用于CO_2还原的新型光电催化装置. 我们最后总结了光电催化CO_2还原目前还面临的问题和此领域今后研究的重点.

